

## Response to Interactive comments from Anonymous Referee #1

Referee comments are in black. Author responses are in blue.

General Remarks: The manuscript present the results of observing NO<sub>2</sub> emission measurements in Beijing based on the Car MAX-DOAS technology. Through 19 times of city-circle-around Car-MAX-DOAS experiments, the author showed the potential of Car MAX-DOAS measurement technology in atmospheric monitoring. This observation method can be effectively used for dynamic monitoring of urban NO<sub>2</sub> emissions. However, the database the authors use for the conclusions is relatively weak. So some revisions are needed to consider this manuscript for publication in ACP.

We thank the anonymous referee for his/her insightful and constructive comments. Below are our point-to-point responses in detail.

### Major concerns:

1. Line 24-25, “typically larger NO<sub>2</sub> VCD at the southern parts of the 6th Ring Road than at the northern parts”. According to Figures 5 and 6, the NO<sub>2</sub> VCD at the southern parts and northern parts were not typically different in January.

The sentence has been deleted in the revised version of the manuscript.

2. Since each measurement time was different, from 2 to 2.5 hours (sometimes nearly 3 hours), the author should introduce the traffic situation during the measurement and analyze the impact on the measurement results.

Traffic jam did not occur during the measurement and the impact of traffic situation should be negligible. Different people might drive at different speeds although we had suggested them to drive at a low speed and stable level. Only after the experiments, we realized that driving slowly might also cause a problem for the emission estimate since the change in wind field might be more pronounced with a longer experimental time.

3. The author should introduce the NO<sub>x</sub> emission sources in Figure 1 and analyze the influence on the measurement.

Because the contribution of transportation to NO<sub>x</sub> emission sources is very large in Beijing, we replace four point sources (Marked as red triangle in Figure 1) with the spatial distribution of total NO<sub>x</sub> emission sources including the transportation, power plant, residential, industry and agriculture sector. We also delete four red triangles in Figure 5, Figure 6, and Figure 8. We have added the related descriptions in lines 199-201 and analyze the influence on the NO<sub>2</sub> VCD measurements in lines 399-401 of the revised manuscript.

4. The results of Car Max- DOAS measurement show that NO<sub>x</sub> emission in heating season is nearly three times as much as that in non heating season, which is obviously higher than that calculated by MEIC inventory estimate. Since central heating is adopted in Beijing urban area, the author should analyze heating season NO<sub>x</sub> sources

in detail, and evaluate the contributions to the measurement results.

Many thanks for suggestions. Central heating from power plant and home heating increase emissions in heating season compared to non-heating season. We calculated the average NO<sub>x</sub> emission rates of four sectors including industry, power, residential, and transportation from the MEIC within the 6th Ring Rd of Beijing in January, September, and October 2012, and the ratio of NO<sub>x</sub> emission rates in Jan. and the average in Sep. and Oct (Table S1). The E<sub>NO<sub>x</sub></sub> from power and residential in January are remarkably higher than other two months, especially E<sub>NO<sub>x</sub></sub> from residential in January are about 5 times those in other months. Corresponding descriptions are added in 374-375 and lines 440-448 of the revised version. We cannot retrieve the specific positions of heating season NO<sub>x</sub> sources from MAX-DOAS measurements by the method used in this study. But we agree that it is a significant scientific issue and will use the source apportionment model to investigate it in the future study.

Minor comments:

1. Abstract, here it is more appropriate to use “different months” instead of “different seasons”.

Corrected.

2. Line 43, “less than” instead of “smaller than”

Corrected.

3. Line 54-56, “NO and NO<sub>2</sub> (together denoted as NO<sub>x</sub>) form primarily in combustion processes, and the conversion between NO and NO<sub>2</sub> in the atmosphere is very rapid” is well known and meaningless here

The sentence has been changed to “the studies on the spatiotemporal variation of NO and NO<sub>2</sub> (together denoted as NO<sub>x</sub>), with the latter being a precursor of nitrate aerosols, are very important for understanding the aerosol formation and its influencing factors” in lines 59-61 of the revised manuscript.

4. Please unify the format of “Car-MAX-DOAS” in the manuscript. For example: line 90 “car-MAX-DOAS”, line 94 “Car-MAX-DOAS”, line 101 “car MAX-DOAS”, line 190 “car MAX-DOAS” et al.

Done.

5. Line 147, “the roof of a car” instead of “the roof a car”.

Corrected.

## Response to Interactive comments from Anonymous Referee #2

Referee comments are in black. Author responses are in blue.

### General Remarks:

The manuscript by Cheng et al. describes mobile-MAX-DOAS measurements of NO<sub>2</sub> VCDs in the Beijing area. The study is based on 19 circuits around the 6th Ring Road in Beijing during two seasons in 2014. Emissions of NO<sub>x</sub> by Beijing were estimated using the MAX-DOAS VCDs as well as winds and NO<sub>x</sub>/NO<sub>2</sub> ratios simulated by the LAPSWRF-CMAQ model system. Simulated winds were validated using wind observations at multiple locations in the region. The seasonal differences between average VCDs and NO<sub>x</sub> emissions were compared and found to be greater during the heating periods. The estimated NO<sub>x</sub> emissions were compared to a bottom-up emission inventory from 2012. The manuscript illustrates how mobile-MAX-DOAS measurements in Beijing and other megacities could provide dynamic monitoring of NO<sub>x</sub> emissions and validation of satellite NO<sub>2</sub> VCDs. My concerns are about the application and interpretation of statistics for the validation of modelled winds (Issue #1), and about the validity of the scientific methods and assumptions for some of the measurement periods and in the calculation of errors (Issue #2), and error calculation (Issue #3). The authors should address the following specific issues and minor corrections before the manuscript is published.

We thank the anonymous referee for his/her insightful and constructive comments. Below are our point-to-point responses in detail.

### Specific Issues:

Issue #1) In general, be careful about application and interpretation of statistics for discussion of means and validation of wind data. Some descriptions of error calculations are not sufficiently complete to allow their reproduction.

Thanks for pointing out this. We have deleted the inappropriate interpretation of statistics for the validation of modelled winds in the revised manuscript.

-Page 2 line 32-33: please include an uncertainty value when stating mean values throughout and, preferably, indicated the statistical type of uncertainty (e.g., standard deviation of mean).

We have added the standard deviation in lines 34-35 of the revised manuscript.

-Page 10 line 266-267: what about Fig. S2 shows that the temporal variation between the simulated and observed wind speed were consistent? An R of 0.47 is quite low given that the R<sup>2</sup>= 0.22, meaning only 22% of variation in the model is explained by variation in the observation. In terms of the simulated wind-speed being greater than the observations, if that conclusion is from the slope being >1, the slope should be assessed with an y-intercept forced to zero. In an ideal case the simulated and observed speeds would be the same (1:1 line, 0 intercept) unless a systematic error or offset is expected.

Also, the slope is barely above zero. Using a linear fitting algorithm program that provides the expected error on the slope and intercept will indicate whether the slope was statistically greater than zero.

We have added a plot showing the time serial of wind speed to the revised supplement (see Fig.4s) and the temporal variation between the simulated and observed wind speed are largely consistent. Although the R of 0.47 is low and there are systematic errors in the modelled wind speed due to impacts of the complex topography and limited observation data assimilated to the LAPS-WRF model, we reduced the error of the modelled wind speed by correction based on measurements at four weather stations in Beijing. In addition, we updated Fig.S2 with an y-intercept forced to zero, and the expected error (standard deviation) of the re-calculated slope calculated with the linear fitting algorithm program is 0.002.

-Page 10 line 268-269: it is still unclear how the relative error was used to “correct” the simulated winds. Did you simply add it as an error bar?

Yes, we added the relative error bar to the simulated wind speed at sampling position of Car MAX-DOAS experiments for each journey. The corresponding descriptions can be seen in lines 322-326 of the revised manuscript.

-Page 10 lines 273-274 The wind rose plots (Fig. S3) give little indication that the wind direction was consistent between the simulation and observations during you driving periods. Without this information, the claim that the modelled winds were accurate is unsupported. Either apply circular statistics to determine the R<sup>2</sup> of simulated and observed wind-directions or provide time series plots of wind-direction (perhaps in the supplemental).

We have given the time series of wind-direction in Fig.S4 in the revised supplement and corresponding description in lines 331-339 of the revised manuscript.

-Page 10 lines 283-284 The regression statistics should be determined using a linear correlation line with an intercept forced to zero (see Page 10 line 266-267 comment).  
Done.

Issue #2) A major assumption of the mobile-MAX-DOAS method for estimating emissions using a flux integral is that winds stayed relatively constant during the measurement period. Therefore, this method is only valid to use on MAX-DOAS data with these wind conditions.

We have skipped over the journeys with the inappropriate wind data and given the error contribution of wind speed and direction to the uncertainty of estimated NO<sub>x</sub> emissions in the revised manuscript.

-Page 14 line 386, point (4): the driving routes should be screened for changing wind field since relatively constant wind fields are a fundamental assumption of Eq. (1) for mobile-MAX-DOAS and, if violated, lead to large, unquantified uncertainties. This point is stated in the manuscript Page 16 lines 444-446 but contrasts with the inclusion

of emission estimates in your figures and comparisons where large wind fluctuations occurred. It is not scientifically valid to use Eq. (1) under these conditions and the emission estimates from these routes should not be presented unless designated as having unknown error.

We excluded the journeys of wind type “O” and given detailed descriptions about the selection process of appropriate wind data for the NO<sub>x</sub> emission estimation in lines 208-221 and lines 351-362 in the revised manuscript. In addition, we have given the error contribution of wind speed and direction to the uncertainty of estimated NO<sub>x</sub> emissions in lines 529-535 of the revised manuscript.

-Page 14 line 395: Therefore, exclude journeys of wind type “other”. See comment above.

Done.

### Issues #3)

-Page 14 line 408-409 The total error values appear too small given all the potential factors contributing to uncertainty. Shaiganfar et al. (2011) suggests that the error of using the VCDgeo calculation alone is up to 20% (<https://doi.org/10.5194/acp-11-10871-2011>). A VCD error 10% is likely too small if both the SCD retrieval error and the VCDgeo errors are combined. Was the error on the simulated wind speed the RMSE between the modelled and observed winds during the driving period? What about the contribution of wind-direction error? If the wind-direction varied a lot, the error contribution would likely dominate.

We re-calculated the NO<sub>x</sub> emissions and its uncertainties using vertical average data of wind speed and direction, the ratio of NO<sub>x</sub> and NO<sub>2</sub>, and the NO<sub>x</sub> lifetime from surface to 1000m at every sampling position on the 6th Ring Rd of Beijing for each journey, and provided updated results of E<sub>NO<sub>x</sub></sub> and corresponding discussions in lines 136-140, lines 159-164, lines 431-440, and lines 506-535 in the revised manuscript. The updated range of emission errors of NO<sub>x</sub> emission is 19.52–52.01%. A VCD error 10% was suggested in the paper of Ma et al., 2013 and used to calculate the uncertainty of E<sub>NO<sub>x</sub></sub>, which seems to be a low limit of VCD errors. We have used the RMSE between the modelled and observed wind speed during the driving period to select appropriate wind data to update the NO<sub>x</sub> emission estimations and adopted the standard deviation to calculate error contributions of wind speed to the uncertainty of E<sub>NO<sub>x</sub></sub>. We have also calculated the contribution of wind-direction error to the estimation of E<sub>NO<sub>x</sub></sub> in Table 3 and given corresponding discussions in lines 529-535 in the revised manuscript. The results show that the error contributions from the wind field dominate, as you expected.

### Minor Issues and Corrections:

Page 2 line 41: replace “consumption” of fossil fuels with “combustion”.

Done.

Page 2 line 47: remove the word “obviously” here and throughout as it is unnecessary.

Done.

Page 2 lines 54-56: since you begin with a discussion of PM, may want to explicitly describe that NO<sub>x</sub> is a precursor of nitric acid, which is a precursor of nitrate aerosols for maximum clarity.

Done.

Page 2 line 60: replace “high” with “large”.

Done.

Page 3 line 64: define “top-down constraint” or use “top-down” emission estimate

We have used the latter.

Page 3 line 71: there is a missing space between sentences.

Corrected.

Page 3 line 72: specify whether it is a large decrease in precision or accuracy?

It is accuracy, incorporated in the revised version.

Page 3 line 74-75: please add citation(s) for these uncertainty factors.

We have added four citations in line 83-84 of the revised version.

Page 3 line 80 MAX-DOAS has been around for nearly two decades (see below).

Hönninger, G. and Platt, U.: Observations of BrO and its vertical distribution during surface ozone depletion at Alert, Atmos. Environ., 36, 2481–2489, [https://doi.org/10.1016/S1352-2310\(02\)00104-8](https://doi.org/10.1016/S1352-2310(02)00104-8), 2002.

Hönninger, G., von Friedeburg, C., and Platt, U.: Multi axis differential optical absorption spectroscopy (MAX-DOAS), Atmos. Chem. Phys., 4, 231–254, <https://doi.org/10.5194/acp-4-231-2004>, 2004.

Wagner, T., Dix, B., von Friedeburg, C., Friess, U., Sanghavi, S., Sinreich, R., and Platt, U.: MAX-DOAS O<sub>4</sub> measurements: A new technique to derive information on atmospheric aerosols – Principles and information content, J. Geophys. Res.-Atmos., 109, D22205, <https://doi.org/10.1029/2004JD004904>, 2004.

We have replaced “the last decade” with “the last two decades” in line 90 of the revised version. All these references have been included in the revised manuscript.

Page 3 line 82: add “pointing” between “zenith” and “directions”

Done.

Page 3 line 82: add “vertical” before “profiles”

Done.

Page 3 lines 84-86: I suggest adding these citations of MAX-DOAS NO<sub>2</sub> measurements (below)

Tan et al. (2018) doi:10.5194/acp-18-15387-2018

Wagner et al. (2011) doi:10.5194/amt-4-2685-2011

Done.

Page 4 line 91: add “horizontal” before “spatial distribution of pollutants” (since the stationary inverse modelling MAX-DOAS technique also gives spatial information but in the vertical).

Done.

Page 4 line 95: in general, you may want to mention that mobile-MAX-DOAS could be very useful for validating the NO<sub>2</sub> VCDs and NO<sub>x</sub> emission estimates from the new, high pixel resolution measurements by the TROPOMI instrument on the Sentinel-5P satellite.

We have added “and validating the NO<sub>2</sub> VCDs and NO<sub>x</sub> emission estimates from the new, high pixel resolution measurements by the TROPOMI instrument on the Sentinel-5P” in lines 101-103 of the revised version.

Page 4 line 105: Consider adding the study objectives or aims before listing the sections. It can help the reader quickly determine if the paper of interest and makes it easier to follow the major conclusions.

We have added the study objectives in lines 116-119 of the revised version.

Page 4 line 115: Please explain why wind-speeds at 10 m above surface was used instead of averaged within the boundary layer height from the model output given can be well-mixed into the boundary layer (up to 600 m in your study) at the location point and, thus, the 10 m wind speed is a lower-bound.

We have re-calculated the NO<sub>x</sub> emissions and its uncertainties using vertical average data of wind speed and direction from surface to 1000m altitude.

Page 5 line 142: The word “mounted” is more appropriate than “settled”.

Corrected.

Page 5 line 143: Please provide information about the instrument specifications (e.g., spectrometer model, spectral resolution, cooling mechanism etc.)

We add the related information in lines 177-183 in the revised manuscript.

Page 6 line: How many measured spectra were averaged to produce a single measurement spectrum?

There were about 200-400 scans typically for each single measurement spectrum. This information has been added to the revised manuscript.

Page 5 line 145: This MAX-DOAS instrument was also used more recently in the Davis et al. (2019) mobile-MAX-DOAS measurements of NO<sub>x</sub> emissions.

We have added the citation in line 175 of the revised version.

Page 6 line 155: Please specify whether the sequence measured multiple 300 spectra or if every 300 measurement was immediately followed by a 900 measurement.

Every 30° measurement was immediately followed by a 90° measurement, and this information has been added to line 192-194 of the revised version.

Page 6 line 164: Please quantify “changed slightly”. Example, the wind changed by <X degrees and < Y m/s during the circle journey.

The description is not appropriate and we have deleted it (lines 204-205 of the revised version). Large wind variability occurred in some journeys and we have added the wind changes of every journey in Table 2.

Page 6 line 175: add “absorption” in front of cross sections.

Done.

Page 6 line 176 typo: “dimmer” should be “dimer”

Corrected.

Page 7 line 185: Do you mean “for in-situ MAX-DOAS measurements”?

Yes, we replace “site” with “in-situ” in line 239 and 248 of the revised version.

Page 7 line 187: Should this be “extending Eq. (6) to Eq. (7)” ?

Corrected.

Page 7 line 194: replace “site” typo with “in-situ”.

Done.

Page 7 line 196: check equation number.

Corrected.

Page 7 Line 197: add (SZA) to DSCD\_offset.

Done.

Page 7 line 204: check the Eq. number.

Corrected.

Page 7 line 205: replace “geometry” with “geometric” and cite Brinksma et al, 2008 <https://doi.org/10.1029/2007JD008808> and Wagner et al. 2010 <https://doi.org/10.5194/amt-3-129-2010>

Done. We have added the citation in line 259 of the revised version.

Page 8 line 209-210: the meaning of this sentence is unclear.

We have revised the sentence.

Page 8 line 211: NO<sub>2</sub> needs subscript.



Corrected.

Page 8 line 215: missing space after “September 23”.

Corrected.

Page 8 line 216: missing period at the end of this sentence.

Corrected.

Page 9 line 233: hyphen needed between “three” and “dimensional”

Done.

Page 9 line 251: delete the extra period.

Done.

Page 10 line 265: change “area” to “areas”

Done.

Page 11 line 294: rewrite the sentence to read “The highest values were between. . .”

The sentence has been rewritten.

Page 11 line 296: see comment for Page 2 line 32-33.

Done.

Page 11 line 300-301: what factors would increase emissions in January compared to October? More home heating?

Central heating from power plant and home heating increase the emissions in January compared to October. We calculated the average NO<sub>x</sub> emission rates of four sectors including industry, power, residential, and transportation from the MEIC within the 6th Ring Rd of Beijing in January, September, and October 2012, and the ratio of NO<sub>x</sub> emission rates in Jan. and the average in Sep. and Oct (Table S1). The E<sub>NO<sub>x</sub></sub> from power and residential are remarkably higher in January than other two months, especially E<sub>NO<sub>x</sub></sub> from residential in January are about 5 times as much as those in other months. In general, central heating is provided in urban area and the scattered coal combustion for heating is popular in suburb or rural area. Corresponding descriptions are added in lines 374-375 and lines 440-448 of the revised version.

Page 11 line 301-302: were lower PBL heights and smaller wind-speeds found in January compared to September/October?

PBL heights and wind speeds in January are not always smaller than September/October. We have deleted the related description in line 375-378 of the revised manuscript.

Page 12 line 337: subscript needed on NO<sub>2</sub> VCD.

Corrected.

Page 12 line 349: see comment for Page 2 line 32-33.

Done.

Page 13 line 371: considering replacing “residents” with “residential”

Done.

Page 13 lines 375-377: in what way does it indicate the applicability? Please explain/elaborate.

The sentence is not correct and has been deleted in lines 471-473 of the revised manuscript.

Page 22 623: fix error in reference name.

Done.

Pages 28 and 29: Figures 5 and 6: correct the unit notation ( $\times 10^{16}$ ) of VCDs in the caption.

Corrected.

Page 31 Figure 8: the caption says “under three types of wind fields” but only south and north winds are shown.

We have replaced “three types” with “two types”.

# Retrieving tropospheric NO<sub>2</sub> vertical column densities around the city of Beijing and estimating NO<sub>x</sub> emissions based on ~~ear~~-Car MAX-DOAS measurements

Xinghong Cheng<sup>1</sup>, Jianzhong Ma<sup>1</sup>, Junli Jin<sup>2</sup>, Junrang Guo<sup>1</sup>, Yuelin Liu<sup>2</sup>, Jida Peng<sup>4</sup>, Xiaodan Ma<sup>5</sup>, Minglong Qian<sup>6</sup>, Qiang Xia<sup>6</sup>, Peng Yan<sup>2</sup>

<sup>1</sup>State Key Lab of Severe Weather & Key Laboratory for Atmospheric Chemistry, Chinese Academy of Meteorological Sciences, Beijing 100081, China

<sup>2</sup>CMA Meteorological Observation Centre, Beijing 100081, China

<sup>3</sup>College of Electronic Engineering, Chengdu University of Information Technology, Chengdu 610225, China

<sup>4</sup>Meteorological Institute of Fujian, Fuzhou 350001, China

<sup>5</sup>Nanjing University of Information Science and Technology, Nanjing 210044, China

<sup>6</sup>China National Huayun Technology Development Corporation, Beijing 100081, China

*Correspondence to:* Xinghong Cheng (cxingh@cma.gov.cn) and Jianzhong Ma (majz@cma.gov.cn)

**Abstract.** We carried out 19 city-circle-around ~~ear~~-Car MAX-DOAS experiments on the 6th Ring Road of Beijing in January, September, and October 2014. The tropospheric vertical column densities (VCDs) of NO<sub>2</sub> were retrieved from measured spectra by the Multi-Axis Differential Optical Absorption Spectroscopy (MAX-DOAS) technique and used to estimate the emissions of NO<sub>x</sub> ( $\equiv$  NO + NO<sub>2</sub>) from urban Beijing during the experimental periods. The offline LAPS-WRF-CMAQ model system was used to simulate the wind fields by assimilation of observational data and calculate the NO<sub>2</sub>-to-NO<sub>x</sub> concentration ratios, both of which are also needed for the estimation of NO<sub>x</sub> emissions. The NO<sub>x</sub> emissions in urban Beijing for the different ~~months~~ seasons derived from the ~~ear~~-Car MAX-DOAS measurements in this study were compared to the multi-resolution emission inventory in China for 2012 (MEIC 2012). Our ~~ear~~-Car MAX-DOAS measurement results showed higher NO<sub>2</sub> VCD in January than in the other two months ~~and typically larger NO<sub>2</sub> VCD at the southern parts of the 6th Ring Road than at the northern parts~~. The wind field had obvious impacts on the spatial distribution of NO<sub>2</sub> VCD, with the mean NO<sub>2</sub> VCD along the 6th Ring Road typically being higher under the south wind than under the north wind. In addition to the seasonal difference, the journey-to-journey variations of estimated NO<sub>x</sub> emissions rates (E<sub>NO<sub>x</sub></sub>) were large even within the same month, mainly due to uncertainties in the calculations of wind speed, the ratio of NO<sub>2</sub> and NO<sub>x</sub> concentration, and the decay rate of NO<sub>x</sub> from the emission sources to the measured positions under different meteorological conditions. The ranges of E<sub>NO<sub>x</sub></sub>

during the heating and non-heating periods were  $22.59 \times 10^{25}$  to  $31.28 \times 10^{25}$   ~~$28.7 \times 10^{25}$  to  $60.0 \times 10^{25}$~~  molecules  $s^{-1}$  and  $9.61 \times 10^{25}$  to  $11.96 \times 10^{25}$   ~~$7.7 \times 10^{25}$  to  $24.8 \times 10^{25}$~~  molecules  $s^{-1}$ , respectively. The average  $E_{NOX}$  values in the heating and non-heating periods were  $26.94 \pm 6.14 \times 10^{25}$  molecules  $s^{-1}$  and  $10.99 \pm 1.23 \times 10^{25}$  molecules  $s^{-1}$ ,  ~~$43.0 \times 10^{25}$  molecules  $s^{-1}$  and  $13.9 \times 10^{25}$  molecules  $s^{-1}$~~ , respectively. The uncertainty range of  $E_{NOX}$  was  ~~$19.52$ – $52.01\%$~~   $16.4$ – $33.2\%$ . The monthly emission rates from MEIC 2012 are found to be lower than the estimated  $E_{NOX}$ , particularly in January. Our results provide important information and datasets for the validation of satellite products and also show how ~~ear~~-Car MAX-DOAS measurements can be used effectively for dynamic monitoring and updating of the  $NO_x$  emissions from megacities such as Beijing.

## 1. Introduction

Over the past decade, serious haze ~~events have~~ ~~weather has~~ occurred frequently in autumn and winter in Beijing due to massive anthropogenic emissions from the ~~combustion~~ ~~consumption~~ of fossil fuels and other sources (He et al., 2013; Zhang et al., 2013). High concentrations of aerosol particulate matter with dynamic diameter ~~less~~ ~~smaller~~ than  $2.5 \mu m$  ( $PM_{2.5}$ ) threaten public health (Cao et al., 2014), disturb traffic operation by affecting visibility, and result in ~~perturbations~~ ~~changes~~ to the weather and climate ~~because of~~ ~~by~~ scattering and absorption of solar radiation (Liao et al., 2015; Cheng et al., 2017). Measurements have shown that organic matter (OM), sulfate, nitrate, and ammonium made up more than 78% of the  $PM_{2.5}$  in January 2013 in Beijing (Huang et al., 2014). Fractions of nitrate in  $PM_{2.5}$  have ~~obviously~~ increased recently with the control of industry and coal in the Beijing-Tianjin-Hebei region, which has reduced  $SO_2$  emissions and the ratio of sulfate in  $PM_{2.5}$ , ~~while traffic emissions are still at high levels. A recent study based on the aerosol observations at the campus of Peking University in 2014 revealed that aerosol pollution is nitrate-driven in spring and early fall and OM-driven in late fall and winter (Tan et al., 2018).~~ ~~Recent research (Tan et al., 2018) based on the aerosol observations at the campus of Peking University in 2014 revealed that aerosol pollution is nitrate driven in spring and early fall and OM driven in late fall and winter.~~ The ~~researchers~~ ~~study~~ suggested that nitrate formation was more significant than sulfate formation during severe pollution episodes in Beijing. Therefore, studies on ~~the spatiotemporal variation of NO and  $NO_2$  (together denoted as  $NO_x$ ), with the latter being a precursor of nitrate aerosols, are very important for understanding the aerosol formation and its influencing factors.~~ ~~the spatiotemporal variation of gaseous precursors of nitrate are very important for understanding~~

~~the aerosol formation and its influencing factors. NO and NO<sub>2</sub> (together denoted as NO<sub>x</sub>) form primarily in combustion processes, and the conversion between NO and NO<sub>2</sub> in the atmosphere is very rapid.~~

Emission inventories are usually developed by the so-called bottom-up approach, which is based on combinations of activity statistics (such as energy consumption and industrial production) and source- or region-specific emission factors (Hao et al., 2002; Zhang et al., 2007; Zhao et al., 2012; Streets et al., 2013). However, there are large high-uncertainties in bottom-up emissions inventories associated with the statistics, emissions factors, temporal allocation profiles, and grid allocation factors (Ma and Van Aardenne, 2004; Zhao et al., 2012). Moreover, estimating “current” emissions by the bottom-up methodology is fundamentally difficult because publication of basic statistics is generally a couple of years behind. The ~~“top-down” emission estimate~~top-down constraint is a useful supplement to bottom-up estimates, which are subject to uncertainties in emissions factors and emissions activities (Streets et al., 2013). Inverse modeling, in which emissions are optimized to reduce the differences between simulated and observed data, is a powerful method that solves the problems of the bottom-up approach. Recently, its application to the estimation of NO<sub>x</sub> emissions has been widely reported. NO<sub>x</sub> emission rates are derived by constraining satellite observations using the relationship between model-simulated NO<sub>2</sub> vertical column density (VCD) and primary NO<sub>x</sub> emission estimates from the bottom-up approach (Martin, 2002; Jaegle' et al., 2005; Konovalov et al., 2006; Wang et al., 2007; Lin et al., 2012; Zyrichidou et al., 2015). Nevertheless, errors and uncertainties still exist in the retrieval of satellite data, ~~and these~~which leads to a large decrease in the accuracy of estimated emissions, precision, particularly in highly polluted regions such as Beijing and its surroundings (Ma et al., 2013a; Jin et al., 2016). Uncertainties can arise from noise, surface albedo, cloud blocks, profile shape, interference from ozone absorption, correlations with other retrieved parameters, fitting wavelength window, and so forth (Jin et al., 2016; Ma et al., 2013a; Shaiganfar et al., 2011, 2017). Air mass factor (AMF) errors can produce additional errors during the conversion process from the slant to vertical columns. Therefore, comprehensive ground-based measurements of the tropospheric columns and vertical profiles of NO<sub>2</sub> are quite important and necessary to evaluate and validate satellite retrieval products.

The Multi-Axis Differential Optical Absorption Spectroscopy (MAX-DOAS)~~MAX-DOAS (Multi-Axis Differential Optical Absorption Spectroscopy)~~ is a new ground-based remote sensing technique developed during the last two decades. It makes use of the scattered sunlight measured from horizontal through zenith pointing direction to retrieve the VCD and vertical profiles of trace gases and aerosols

with relatively high sensitivity in the lower atmosphere (Hönninger et al., 2004; Wagner et al., 2004; Platt and Stutz, 2008). MAX-DOAS has been extensively used to derive tropospheric column information of NO<sub>2</sub> and some other pollutants in various regions (Wittrock et al., 2004; Brinksma, et al., 2008; Irie et al., 2008; Vlemmix et al., 2010; Li et al., 2013; Hendrick et al., 2014; [Tan et al., 2008; Wagner et al., 2011](#)). Mobile- (or ~~ear~~Car-) MAX-DOAS measurements have been used to quantify NO<sub>x</sub> emissions from cities and regions such as Beijing (Johansson et al., 2008), Mexico (Johansson et al., 2009), Mannheim and Ludwigshafen (Ibrahim et al., 2010), Deli (Shaiganfar et al., 2011), Shanghai (Wang et al., 2012), North China (Wu et al., 2018). Compared to ground-based observations at a fixed site, ~~ear~~Car-MAX-DOAS measurements can provide information on the [horizontal](#) spatial distribution of pollutants, which is important for explaining the urban/regional representativeness of satellite observations [and validating the NO<sub>2</sub> VCDs and NO<sub>x</sub> emission estimates from the new, high pixel resolution measurements by the TROPOMI instrument on the Sentinel-5P](#) over megacities such as Beijing. Moreover, due to the rapid expansion of urban area and increasing energy consumption, both locations and strength of emission sources in Beijing ~~might may~~ have changed significantly. Therefore, intensive Car-MAX-DOAS measurement campaigns are still needed to estimate the emissions of NO<sub>x</sub> in Beijing. Mean wind speed and wind direction along the ring road during the sampling periods ~~were are~~ usually used to estimate NO<sub>x</sub> emissions in ~~the~~ previous studies. Since wind field changes rapidly due to local circulation and then results in uncertainties in quantification of NO<sub>x</sub> emissions (Johansson et al., 2008; Shaiganfar et al., 2011, 2017; Davis, et al., 2019), refined and accurate simulations of wind fields are needed for the accurate emission estimate.

In this study, we estimated the total NO<sub>x</sub> emissions from urban Beijing based on the VCD of NO<sub>2</sub> obtained from intensive ~~ear~~Car MAX-DOAS measurements on the 6th Ring Road of Beijing in January, September, and October of 2014. The offline LAPS-WRF-CMAQ model system with data assimilation method was used to derive wind speed, wind direction, and NO<sub>2</sub>/NO<sub>x</sub> concentration ratios, which are needed to estimate total urban NO<sub>x</sub> emissions based on ~~ear~~Car MAX-DOAS measurements. [We attempted to accurately estimate the NO<sub>x</sub> emission rates and the seasonal difference and deeply investigate the uncertainties and appropriate meteorological conditions for the estimation based on Car MAX-DOAS measurements.](#) This paper is organized as follows: Section 2 describes the intensive ~~ear~~Car MAX-DOAS experiments and the retrieval method for deriving tropospheric NO<sub>2</sub> VCD, the model system used to simulate ~~the~~ wind fields and the ratios of NO<sub>2</sub> and NO<sub>x</sub>, and the method used to quantify

total NO<sub>x</sub> emissions. Section 3 presents the results of the NO<sub>2</sub> VCD and the estimated NO<sub>x</sub> emissions as well as their uncertainties due to simulated errors in the wind field. Conclusions are provided in Section 4.

## 2. Theory, experimental, and method

### 2.1 Formula to estimate urban NO<sub>x</sub> emissions

The complete NO<sub>2</sub> flux  $F_{NO_2}$  across the urban Beijing area encircled by the driving route  $S$  is estimated according to the closed integral method (CIM)~~the method~~ of Ibrahim et al. (2010).

$$F_{NO_2} = \oint_S VCD_{NO_2}(s) \cdot \vec{w} \cdot \vec{n} \cdot ds \quad (1)$$

Here  $VCD_{NO_2}(s)$  is the NO<sub>2</sub> VCD at the sampling position within the driving route;  $\vec{n}$  indicates the normal vector parallel to the Earth's surface and orthogonal to the driving direction at the position of the driving route;  $\vec{w}$  is the average wind vector within the NO<sub>2</sub> layer, which is denoted by wind speed at the height of 10 m. We carried out ~~car~~ Car MAX-DOAS measurements along closed driving routes around large emissions sources, i.e., the 6th Ring Road of Beijing (Fig. 1).

We averaged the wind vector data from the WRF model between surface and 1000m altitude weighted by the winter exponentially decreasing profiles according to the method of Shaiganfar et al. (2017).

$$\vec{w} = \frac{\sum_i w(z_i) \cdot e^{-\frac{z_i}{z_0}}}{\sum_i e^{-\frac{z_i}{z_0}}} \quad (2)$$

Here  $w(z_i)$  is the wind vector at altitude  $z_i$ , and  $z_0$  indicates the assumed scale height of 300m for winter.

According to the ~~calculation method of Ibrahim et al. (2010)~~ CIM, the complete NO<sub>x</sub> emissions from the encircled areas are determined considering the partitioning between NO and NO<sub>2</sub> ( $c_L$ ) and the finite lifetime of NO<sub>x</sub> ( $c_\tau$ ).

$$E_{NO_x} = c_L \cdot c_\tau \cdot F_{NO_2} \quad (23)$$

$$c_L = \frac{c_{NO_x}}{c_{NO_2}} \quad (34)$$

Here  $c_L$  is simply the ratio of NO<sub>x</sub> ( $C_{NO_x}$ ) and NO<sub>2</sub> ( $C_{NO_2}$ ) bulk concentration in the polluted layer which are simulated by the CMAQ model in this study. It is a function of the Leighton ratio ( $L_c = [NO]/[NO_2]$ ),  $c_L = 1 + L_c$ . To analyze whether there is or not the impact of VOCs on lifetime of NO<sub>x</sub>, we also calculate another Leighton ratios,  $L_r$ , referring to the method of Davis et al. (2019).

$$L_r = \frac{j_{NO_2}[NO_2]}{k_8[NO][O_3]} \quad (5)$$

Where  $j_{NO_2}$  is the  $NO_2$  photolysis rate,  $k_8$  is the temperature-dependent rate constant for the reaction between NO and  $O_3$ . We calculate  $j_{NO_2}$  according to the method of Dickerson et al., 1982

$c_\tau$  describes the decay of  $NO_x$  from the emission sources to measured positions.  $c_\tau$  can be estimated from the  $NO_x$  lifetime  $\tau$ , which is the reciprocal of the product of reaction rate constant  $k$ , OH concentration ( $C_{OH}$ ) and air density ( $M$ ) (Ma et al., 2013), and transport time  $t$ , which is the distance between emission source and sampling point  $r$  divided by the wind speed  $\vec{w}$ .

$$c_\tau = e^{\frac{t}{\tau}} = e^{\frac{r/\vec{w}}{\tau}} \quad (46)$$

$$\tau = \frac{1}{k * C_{OH} * M} \quad (47)$$

We firstly calculated averaged simulated wind speed and direction, the ratio of  $NO_x$  and  $NO_2$ , and the  $NO_x$  lifetime from surface to 1000m at every sampling position on the 6th Ring Rd of Beijing for each journey, and computed the distance between the sampling position and the center of the city of Beijing for  $r$ . Then, we computed the  $c_\tau$ ,  $F_{NO_2}$ , and  $E_{NO_x}$ . The lifetime  $\tau$  was calculated with simulated average OH concentration and air density from surface to 1000m at each sampling position for each journey.

We averaged our model simulated quantities over the urban area for the  $NO_x$  lifetime  $\tau$ , used the simulated wind speed at sampling position as  $w$ , and computed the distance between the sampling position and the center of the city of Beijing for  $r$ .

## 2.2 Car MAX-DOAS measurements

### 2.2.1 Instrument and experiment

We measured and retrieved tropospheric  $NO_2$  VCD along the sixth ring road of Beijing (hereafter referred to as 6th Ring Rd) in January, September, and October of 2014 using a Mini MAX-DOAS instrument mounted on the vehicle.

The instrument, manufactured at Hoffmann Messtechnik GmbH, Germany, is a fully automated, light-weighted spectrometer designed for the spectral analysis of scattered sunlight by the MAX-DOAS technique (Hönninger et al., 2004; Davis et al., 2019). The same type of instrument was used in previous studies, including long-term site measurements in Beijing (Ma et al., 2013a) and a car MAX-DOAS observational journey in Europe (Wagner et al., 2010a). The instrument consists of a hermetically sealed



metal box of approximately 3 liter volume containing entrance optics, fiber coupled spectrograph and all electronics. A spectrometer with the model Ocean Optics USB2000+ is used. A stepper motor, adjusted outside the box, rotates the whole instrument to control the elevation viewing angle. The spectrograph covers the range 292-436 nm and its entrance slit is 50  $\mu\text{m}$  wide. A Sony ILX511 CCD (charged coupled device) detects the light in 2048 individual pixels. The whole spectrograph is cooled by a Peltier stage to guarantee a stable temperature of the optical setup and a small dark current signal. For this study, the instrument was mounted on the roof of a car. Inside the car, two 12V DC batteries alternatively supplied electronic power for the running of instruments and a laptop computer, with a script run by the DOASIS software (Kraus, 2001b) to control the measurement process and the recording of spectra. The temperature of the spectrograph was set to be maintained at  $-5^{\circ}\text{C}$  in January and at  $0^{\circ}\text{C}$  in September and October, well below the ambient temperatures during the experimental days of the study. The signal spectra of dark current and electronic offset were measured each day before and after the field experiment on the road, with 10000 msec and 1 scan for dark current measurements and 3 msec and 1000 scans for electronic offset measurements. Measurements were made alternatively at  $30^{\circ}$  and  $90^{\circ}$  elevation angles, with every  $30^{\circ}$  measurement immediately followed by a  $90^{\circ}$  measurement. Each elevation angle measurement had an integration time of about 1 min, including typically 300-400 scans for an average spectrum. ~~with an integration time of about 1 min for each elevation angle.~~

The instrument onboard the car was operated to measure scattered sunlight from the driving forward direction. There were no high buildings on both sides of the 6th Ring Rd., and the measurements were made at a wide-field view. The driving speed was typically controlled at  $80\text{--}90\text{ km h}^{-1}$ , and it generally took about 2.0–2.5 h to complete one circle (about 187 km) around the 6th Ring Rd. Figure 1 shows the driving route of the ~~car~~ Car MAX-DOAS experiment on a map of Beijing and spatial distribution of the yearly  $\text{NO}_x$  emission rate with a resolution of  $0.25^{\circ} \times 0.25^{\circ}$  from the MEIC inventory in 2012, which includes transportation, power plant, residential, industry and agriculture. For this study, the field experiments were carried out on 14 selected days, with one or two circling ~~circle~~ journeys each day. In total, there are 19 circling journeys available. The sampling periods in this experiment and the meteorological conditions are listed in Table 1. ~~In most cases, the meteorological conditions changed slightly within one circling journey period.~~ The average wind speeds for experimental days in January, September, and October were 2.5, 2.5, and  $2.4\text{ m s}^{-1}$ , the corresponding total cloud fractions were 4.9, 7.5, and 4.2, and the mean planetary boundary layer (PBL) heights were 192, 188, and 238 m, respectively.

The dominant wind directions in the three months were much more variable, including north, south, ~~and other directions~~, other directions, and static wind field. Since variations of wind field can affect the estimation of  $E_{\text{NO}_x}$ , we synthetically analyze distribution of wind field using simulations from the WRF model and reanalysis data with a spatial resolution of  $0.125^\circ \times 0.125^\circ$  every three hours from the European Centre for Medium-Range Weather Forecasts (ECMWF). In some cases, the wind direction changed slightly within one circling journey period which is marked as south (S) or north (N) type in Table 1. However, the wind field during some journeys was convergent or divergent in some areas of Beijing which is marked as other type (O), and the wind speed was very low in three journeys which is marked as static type (St). To estimate the NO<sub>x</sub> emissions accurately using the CIM, the wind speed needs to be sufficiently high so that the transport across the encircled area is fast compared to the atmospheric lifetime of the trace gas (Ibrahim et al., 2010). In this study, we only consider the circling journeys with consistent wind field (S or N type) and relatively high wind speed to estimate the NO<sub>x</sub> emissions. The primary information for all the journeys, including 11 selected ones for emission estimation, is given in Table 1.

### 2.2.2 Spectral retrieval

The retrieval of NO<sub>2</sub> slant column densities (SCDs) is based on the DOAS method (Platt, 1994). The WinDOAS software (Fayt and Van Roozendael, 2011) was adopted to analyze the spectra in the 400-431 nm range on a daily basis. The Fraunhofer reference spectrum (FRS) was selected among the measured spectra at the 90° elevation angle each day by two steps: first, a spectrum measured around noon was chosen; second, the spectrum corresponding to the minimum NO<sub>2</sub> SCD derived in the preliminary analysis using the FRS from the first step was finally selected. The absorption cross sections of NO<sub>2</sub> at 294 K (Vandaele et al., 1998), O<sub>3</sub> at 221 K (Burrows et al., 1999), and the Oxygen dimer ~~dimmer~~-O<sub>4</sub> at 298 K (Greenblatt et al., 1990), as well as a FRS, a Ring spectrum calculated from the FRS by DOASIS (Kraus, 2001a) and a polynomial of third order were included in the spectral fitting process. Figure 2 shows an example of our spectral analysis for a measurement on 18 January 2014, 11:39:38 BJT. As shown in the figure, the atmospheric NO<sub>2</sub> absorption structure can be clearly extracted from the measured spectra.

### 2.2.3 Derivation of tropospheric NO<sub>2</sub> VCD

The trace gas VCD in the troposphere can be calculated using its SCD divided by the air mass factor (AMF) at an elevation angle,  $\alpha$ :

$$VCD_{\text{trop}} = \frac{SCD_{\text{trop}}(\alpha)}{AMF_{\text{trop}}(\alpha)} \quad (68)$$

For the ~~in-situ site~~ MAX-DOAS measurements, a FRS from the same elevation sequence was used in most cases, and the stratospheric absorption can be assumed to be the same during one elevation sequence. Therefore, the  $VCD_{\text{trop}}$  can be calculated by extending Eq. 48 to Eq. 29 using the so-called differential tropospheric slant column density ( $DSCD_{\text{trop}}(\alpha) = SCD_{\text{trop}}(\alpha) - SCD_{\text{trop}}(90^\circ)$ ) divided by the differential air mass factor ( $DAMF_{\text{trop}}(\alpha) = AMF_{\text{trop}}(\alpha) - AMF_{\text{trop}}(90^\circ)$ ):

$$VCD_{\text{trop}} = \frac{DSCD_{\text{trop}}(\alpha)}{DAMF_{\text{trop}}(\alpha)} = \frac{DSCD_{\text{meas}}(\alpha)}{DAMF_{\text{trop}}(\alpha)} \quad (79)$$

with  $DSCD_{\text{meas}}(\alpha) = SCD_{\text{meas}}(\alpha) - SCD_{\text{ref}}$  (Wagner et al., 2010b; Ma et al., 2013a).

For the ~~ear-Car~~ MAX-DOAS measurements, the trace gas concentrations can change significantly during one measurement sequence and thus the dependence of retrieved trace gas DSCDs on the elevation angle may not be so regular as for the ~~in-situ site~~ measurements. Therefore, it would be a better choice to use a single FRS for the analysis of all the spectra measured along the driving route (Wagner et al., 2010b). According to Wagner et al. (2010b), Eq. 49 can be further extended to

$$VCD_{\text{trop}} = \frac{DSCD_{\text{meas}}(\alpha) - DSCD_{\text{offset}}(SZA)}{AMF_{\text{trop}}(\alpha)} \quad (108)$$

where  $DSCD_{\text{offset}}$  depends on the solar zenith angle (SZA) and thus local time,  $t_i$ . For each elevation sequence  $i$  during the individual measurement day,  $DSCD_{\text{offset}}$  is calculated from a single pair of measurements with

$$DSCD_{\text{offset}}(t_i) = \frac{AMF_{\text{trop}}(90^\circ) \cdot DSCD_{\text{meas}}(\alpha, t_i) - AMF_{\text{trop}}(\alpha) \cdot DSCD_{\text{meas}}(90^\circ, t_i)}{AMF_{\text{trop}}(\alpha) - AMF_{\text{trop}}(90^\circ)} \quad (119)$$

The time series of the calculated  $DSCD_{\text{offset}}(t_i)$  in this study could be fitted by a low-order polynomial, e.g.,  $P(x) = a_0 + a_1 \cdot x + a_2 \cdot x^2$ , as a function of time. The fitted polynomial then represents the best guess for  $DSCD_{\text{offset}}$  and can be used to calculate the  $VCD_{\text{trop}}$  from Eq. 103. In this study, the AMF was calculated by the ~~geometric geometry~~ approximation (Brinksma et al., 2008; Wagner et al., 2010b), that is:

$$AMF_{\text{trop}}(\alpha) \approx \frac{1}{\sin(\alpha)} \quad (124)$$

As an illustration, Figure 3 shows the changes of individual  $NO_2$   $DSCD_{\text{meas}}$  and  $DSCD_{\text{offset}}$  for  $30^\circ$  elevation angle of each sequence as a function of time on 18 January 2014. As shown in Fig. 3, a second

order polynomial fitted from individual  $DSCD_{offset}$  data points as shown in Fig. 3 tends to be stable and  
265 can be used to represent an average value of  $DSCD_{offset}$ . tends to converge against a much more stable  
average  $DSCD_{offset}$  value.

#### ~~2.2.4 Calculation of monthly average $NO_2$ VCD~~

### 2.3 LAPS-WRF-CMAQ model simulation

#### 2.3.1 Model setup and data

270 To quantify the  $NO_x$  emissions in Beijing more accurately, refined simulations of the wind field and  $NO_2$   
to  $NO_x$  concentration ratio were needed. In this study, we utilized the offline LAPS-WRF-CMAQ model  
system with high spatiotemporal resolution and data assimilation technique to obtain the refined wind  
speed and wind direction and an accurate ratio of  $NO_2$  and  $NO_x$  concentration during the ~~ear~~-Car MAX-  
DOAS experiments. The aforementioned model system includes three components: the LAPS model  
275 (Albers et al., 1996), the WRF model (Michalakes et al., 2004), and the CMAQ model (Dennis et al.,  
1996). Simulation of wind speed and direction is improved by the LAPS-WRF model, which assimilates  
observed data at the surface and high layers using the one-dimensional and three-dimensional variational  
assimilation method (Albers et al., 1996). The CMAQ model is used to simulate temporal-spatial  
distribution of  $NO_2$  and  $NO$  concentration. The Local Analysis and Prediction System (LAPS), developed  
280 by the NOAA Earth System Research Laboratory, is used in many numerical weather forecast centers  
around the world. It is a mesoscale meteorological data assimilation tool that employs a suite of  
observations to generate a realistic, spatially distributed, time-evolving, three-dimensional representation  
of atmospheric features and processes (McGinley et al., 1991). The three-dimensional realistic  
meteorological analyses field can be used as the initial condition of the WRF model and improve the  
285 simulation of wind field. WRF is a mesoscale numerical weather prediction system designed for both  
atmospheric research and operational forecasting needs. CMAQ is an air-quality model developed by the  
U.S. Environmental Protection Agency's Atmospheric Science Modeling Division. It consists of a suite  
of computer programs for modeling air quality issues, including reactive gases such as  $NO_2$ ,  $NO$ ,  $SO_2$ ,  
 $O_3$ , and others, particulate matter (PM), air toxics, acid deposition, and visibility degradation.

290 This study focused on Beijing at a horizontal resolution of  $4\text{ km} \times 4\text{ km}$  with 31 vertical layers of  
varying thickness (between the surface and 50 hPa) using a triple-nested simulation technique. The  
horizontal resolutions of the three sets of grids were 36 km, 12 km, and 4 km, respectively (Fig. S1a),

and the output temporal interval was 1 h. The LAPS-WRF simulations were driven by FNL/NCEP analysis data every 6 h during the ~~ear~~Car MAX-DOAS experiments, with a spatial resolution of  $1^\circ \times 1^\circ$ .

In addition, to improve the simulation of wind field and  $\text{NO}_2$  and NO concentrations, many meteorological data of the same periods, such as wind speed, wind direction, air temperature, and relative humidity, observed at 2400 surface weather stations and by 120 radiosonde stations were assimilated into the initial field of the WRF model using the one-dimensional and three-dimensional variational assimilation method in the LAPS model. The CMAQ model uses the multi-resolution emission inventory in China for the year 2012 (MEIC 2012)~~MEIC 2012~~ with  $0.25^\circ \times 0.25^\circ$  resolution (Zhang et al., 2009; Li et al., 2017). Hourly gridded MEIC emission datasets at a horizontal resolution of  $4 \text{ km} \times 4 \text{ km}$  for the CMAQ model were generated by the Sparse Matrix Operator Kernel Emissions (SMOKE) modeling system (UNC, 2014) using reasonable temporal and spatial allocation coefficients (Cheng et al., 2017). Meteorological outputs from the WRF simulations were processed to create model-ready inputs for CMAQ using the Meteorology–Chemistry Interface Processor (MCIP) (Otte and Pleim, 2010). The chemical mechanism is CB05, and the boundary conditions of trace gases consist of idealized, Northern Hemispheric, mid-latitude profiles based on results from the NOAA Agronomy Lab Regional Oxidant Model. The model simulation was started one day before the first day of the experiment to avoid the spin-up problem and improve the simulation accuracy.

### 2.3.2 Validation of simulated surface wind and $\text{NO}_2$

Modelled wind speeds and directions were validated by observation data from four weather stations in Beijing. Figures S2, S3 and S4 show the scatter distribution between simulated wind speed and observation, wind rose of modelled wind direction and measurements, and their time serials. We adopted the ~~The~~ observed hourly wind speed and direction data ~~at the meteorological stations, shown in Figures S2 and S3, were obtained from the China Meteorological Administration. The four stations are the~~ from Nanjiao (NJ), Tongzhou (TZ), Mentougou (MTG), and Shunyi (SY) meteorological stations, which represent the south, east, west, and north areas of Beijing, respectively. It was shown that the temporal variation in simulated wind speed at the four stations were consistent with the observations from the perspective of time serial of wind speed, but the simulations were higher than the observations due to impacts of the complex topography and limited observation data assimilated to the LAPS-WRF model (Fig. S2 and Fig. S4a)~~(Fig. S2)~~. To calculate the  $E_{\text{NO}_X}$  accurately, we corrected the simulated wind

speed using the observation data from the four weather stations in order to reduce the systemic error. Specifically, we computed the relative error of the modeled wind speed based on measurements at four weather stations for each journey and then added the error bar to simulated wind speed at every sampling position during the same journey. we computed the relative error of modelled wind speed during every journey and then used it to correct the simulated wind speed at all sampling points for every journey. The correlation coefficient between simulated and observed wind speeds at the four stations ~~was-is~~ 0.47, and the result ~~passespassed~~ the 99.9% significance test. The root mean square error (RMSE) ~~was-is~~ small, with a value of  $1.18 \text{ m s}^{-1}$ . Except for the MTG station, simulated wind directions at the other three stations ~~are were~~ in accordance with the observations, particularly for the primary wind direction (Fig. S3 and Fig.S4b). In general, simulated wind direction are also coincident with observations from the perspective of time serial of wind direction, and simulations are larger than measurements during some periods at some stations due to the effects of the complex topography and limited observation data assimilated to the model (Fig.S4b). The primary wind direction and its frequency at the MTG station ~~were-are~~ not consistent with the observations because these are affected by the complex topography near the Taihang and Yanshan mountains. In general, the corrected wind speed and wind direction data are reliable for estimation of the  $\text{NO}_x$  emissions, and the uncertainty of  $E_{\text{NO}_x}$  due to the variation of wind field will be discussed in Section 3.3. Hence, the simulations of wind speed and wind direction were reliable for estimation of the  $\text{NO}_x$  emissions.

Figure S4 presents the temporal variation in simulated and observed  $\text{NO}_2$  concentration from January 18 to October 13, 2014. The hourly measurements of  $\text{NO}_2$  concentrations (shown in Fig. S1b) were obtained from the National Environment Monitoring Station in China. In general, the temporal variation in the  $\text{NO}_2$  simulation ~~was-is~~ consistent with the observation. The simulated values ~~were-are~~ close to the observations, except for January 21–24, September 19, and October 9–10, when  $\text{NO}_2$  simulations ~~were~~ are higher than the observations. The correlation coefficient between simulated and observed  $\text{NO}_2$  concentrations ~~was-is~~ 0.73, and the result ~~passes passed~~ the 99.9% significance test (Fig. S5). The RMSE and mean absolute error (MAE) ~~were-are~~ 16.14 and  $19.21 \mu\text{g m}^{-3}$ , respectively. ~~Because-The~~ observed  $\text{NO}_2$  might include ~~the-some~~  $\text{NO}_z$  component, ~~it-can-lead~~ leading to a systematical biases (underestimation) of  $\text{NO}_2$  by model compared to observation (Ma et al., 2012). Thus, the simulated  $\text{NO}_2$  concentrations and hence the ratio of  $\text{NO}_2$  and  $\text{NO}_x$  ~~were-are~~ reliable for estimating  $\text{NO}_x$  emissions.

## 2.4 Selection of the journeys for estimating NO<sub>x</sub> emissions

To estimate the NO<sub>2</sub> fluxes ( $F_{\text{NO}_2}$ ) and  $E_{\text{NO}_x}$  accurately, we firstly selected six journeys with the RMSEs of simulated wind speeds at the four weather stations smaller than  $1.5 \text{ m s}^{-1}$  from the primary selected 11 journeys. Then we assessed whether the meteorological and chemical conditions meet the criteria of Shaiganfar et al. (2017) for each of these six journeys. It should be pointed out that we cannot assess the problem of large partitioning ratio due to the absence of the whole seasonal simulated or observed data in autumn and winter. The assessment results of other four problems are listed in Table 2. We excluded the journeys in which more than two problems occurred. It needs to be noted that lifetime correction coefficients  $c_t$  on October 12 and 13 are slightly larger than 1.5, which is the criteria of large lifetime correction (Shaiganfar et al., 2017), so we also adopted the data on October 12 and 13 to estimate the  $E_{\text{NO}_x}$ . Lastly, NO<sub>2</sub> VCD measurements outside of the 6th Ring Rd during five selected journeys were not used to quantify  $F_{\text{NO}_2}$  and  $E_{\text{NO}_x}$ .

## 3. Results and discussion

### 3.1 Tropospheric NO<sub>2</sub> VCD

Figure 4 presents the journey-to-journey temporal variation in the tropospheric NO<sub>2</sub> VCD on the 6th Ring Rd of Beijing in January, September, and October, 2014. In general, the NO<sub>2</sub> VCD in January was higher than that in other months. The highest values ~~falling between  $8 \times 10^{16}$  and  $13 \times 10^{16}$  molecules  $\text{cm}^{-2}$~~  occurred on January 19, 23, and 24. ~~The mean, maximum, and minimum NO<sub>2</sub> VCD during the sampling periods were all larger in January than in the other two months.~~ The mean NO<sub>2</sub> VCD ranged mostly from  $4.5 \pm 1.83 \times 10^{16}$  to  $9.0 \pm 1.24 \times 10^{16}$   ~~$4.5 \times 10^{16}$  to  $9 \times 10^{16}$~~  molecules  $\text{cm}^{-2}$  in January, but values were all lower than  $4.5 \times 10^{16}$  molecules  $\text{cm}^{-2}$  in September and October. The NO<sub>2</sub> VCD values during the mornings of January 23 and October 13 were  $9.05 \times 10^{16}$  and  $1.23 \times 10^{16}$  molecules  $\text{cm}^{-2}$ , corresponding to the maximum and minimum values, respectively, during the 19 circling journeys. This result ~~may~~ might be caused by higher emissions from coal fired heating (Table S1) and lower photolysis of NO<sub>2</sub> in winter. ~~and some meteorological conditions that were unfavorable for dispersion and transport of pollutants in winter. Lower PBL height and lower wind speed suppress horizontal and vertical diffusion and transport of NO<sub>x</sub>. Southwest and east winds are favorable for the transport of air pollutants from the south and east areas to the city of Beijing. Higher cloud cover is unfavorable for photolysis of NO<sub>2</sub>.~~ A similar pattern of seasonal variation in tropospheric NO<sub>2</sub> VCD was found previously by site MAX-DOAS

measurements in Beijing (Ma et al., 2013a; Hendrick et al., 2014).

To investigate the differences in the spatial distribution of NO<sub>2</sub> VCD among the three months, we computed the monthly average NO<sub>2</sub> VCD for every sampling point along the 6th Ring Rd of Beijing in January, September, and October, 2014. Firstly, we used the locations of all sampling points on the morning of September 23 as the reference point for the calculation of NO<sub>2</sub> VCD monthly average, with the most sampling sites (98 points) for all observation periods. Then, we calculated the monthly average value at each reference point using the data of the nearest sampling point. The distance from the nearest sampling point to a reference point was less than 1.5 km. Figure 5 shows that the monthly average NO<sub>2</sub> VCD values at most sampling points on the 6th Ring Rd were obviously ~~higher~~ larger in January than in ~~the~~ other two months (by a factor of two in most cases). The spatial distribution characteristics of NO<sub>2</sub> VCD in September were similar to those in October. In addition, the NO<sub>2</sub> VCD values at the northern and southern parts of the 6th Ring Rd were all larger than those in other areas for all three months. The high NO<sub>2</sub> VCD in the southern region was related to strong local emissions to the south of Beijing and transport from central and southern Hebei and the city of Tianjin (Meng et al., 2018).. As shown in Fig. 4, the maximum journey-averaged NO<sub>2</sub> VCD occurred on the morning of January 23, and the minimum occurred on the morning of October 13.

We investigated the spatial distribution differences in NO<sub>2</sub> VCD between these two circling journeys, as shown in Fig. 6. The NO<sub>2</sub> VCD values on the 6th Ring Rd in the morning of January 23 were all large, particularly in the north and southwest areas, with magnitudes of  $10 \times 10^{16}$  to  $12 \times 10^{16}$  molecules cm<sup>-2</sup>. On October 13, high NO<sub>2</sub> VCD was located ~~in at~~ the southern areas and it might be related to the southern emission sources closer to the south 6th Ring Rd, which its emission rates are obviously higher than the north Ring Rd., ~~but values were lower in the northern areas.~~ The spatial distribution differences between these two journeys were related to the high emission during the heating season in January (see section 3.2) and the impacts of the wind field. ~~To investigate the impact of the wind field on the spatial distribution of NO<sub>2</sub> VCD, we~~ We used thin-grid ECWMF reanalysis data for January 23 and October 13 with a spatial resolution of  $0.125^\circ \times 0.125^\circ$  to investigate the impact of the wind field on the spatial distribution of NO<sub>2</sub> VCD. Figure 7 shows the ~~distribution difference of~~ wind fields at 8:00 and 14:00 BJT on these two days, respectively. The NO<sub>2</sub> VCD was large with weak south wind and ~~with~~ convergence of southeast and northwest wind in Beijing and its surrounding area, but its values were far smaller with strong north wind. Weak south wind and a breeze or calm wind resulted in the transport of NO<sub>2</sub> from the



south area in Hebei Province and its accumulation on January 23. Strong north wind suppressed the transport of NO<sub>2</sub> from the south area on October 13. These results indicate that the wind field has large impacts on the spatial distribution of NO<sub>2</sub> VCD in Beijing.

Figure 8 presents the spatial distributions of wind and NO<sub>2</sub> VCD averaged for the ~~three~~-two different wind fields. The mean NO<sub>2</sub> VCD at most sampling points along the 6th Ring Rd was obviously higher under the south wind field than under the north wind. High NO<sub>2</sub> emission ~~in the three months was~~ sources were located within the 5th Ring Rd of Beijing in the three months (Fig. 10), and the background concentrations of NO<sub>2</sub> VCD in the north and south areas were remarkably different due to the impacts of emission sources ~~from to the south areas of Beijing, such as Hebei Province~~. Hence, southerly wind can transfer air pollutants from the southern area to Beijing and lead to high NO<sub>2</sub> flux ~~and NO<sub>x</sub> emission~~, whereas impacts of north wind on NO<sub>2</sub> flux ~~and NO<sub>x</sub> emission~~ are smaller because the background concentration of NO<sub>2</sub> VCD ~~in to the north of Beijing is~~ were lower. Convergence of the wind field in the south parts of the 6th Ring Rd is favorable to the accumulation of NO<sub>2</sub> from the surrounding area to the southern parts of the ring road.

### 3.2 Quantification of NO<sub>x</sub> emissions

~~Figure 9 shows the journey-to-journey variation in estimated F<sub>NO2</sub> and E<sub>NOX</sub> over Beijing for five circling journeys in January, September, and October, 2014. To estimate the NO<sub>2</sub> fluxes (F<sub>NO2</sub>) and E<sub>NOX</sub> accurately, we used the data from 10 circling journeys (Table 1), for which the RMSEs of simulated wind speeds at the four weather stations were all less than 1.5 m s<sup>-1</sup>. In addition, NO<sub>2</sub> VCD measurements at the sampling points outside of the 6th Ring Rd during 11 circling journeys were not used to quantify F<sub>NO2</sub> and E<sub>NOX</sub>.~~ Figure 9 shows the journey to journey variation in estimated F<sub>NO2</sub> and E<sub>NOX</sub> over Beijing for the 10 circling journeys in January, September, and October, 2014. The F<sub>NO2</sub> fell in between ~~1.85~~1.13 × 10<sup>25</sup> and ~~11.35~~15.67 × 10<sup>25</sup> molecules s<sup>-1</sup>. The ranges of E<sub>NOX</sub> during the heating (January) and non-heating (September and October) periods were ~~28.7~~22.59 × 10<sup>25</sup> to ~~60.0~~31.28 × 10<sup>25</sup> molecules s<sup>-1</sup> and ~~7.79~~6.1 × 10<sup>25</sup> to ~~24.8~~11.96 × 10<sup>25</sup> molecules s<sup>-1</sup>, respectively. The average E<sub>NOX</sub> values in the heating and non-heating periods were ~~26.94 ± 6.14~~43.0 × 10<sup>25</sup> molecules s<sup>-1</sup> and ~~10.99 ± 1.23~~13.9 × 10<sup>25</sup> molecules s<sup>-1</sup>, respectively. In general, the journey-to-journey variation patterns of F<sub>NO2</sub> and E<sub>NOX</sub> ~~were~~ are consistent with that of the mean NO<sub>2</sub> VCD. In other words, the estimate of E<sub>NOX</sub> ~~was~~ is determined mainly by the NO<sub>2</sub> VCD. Seasonal variation characteristics of the estimated E<sub>NOX</sub> were obvious.

Specifically, the total  $E_{NOX}$  was higher in January than in the other two months. The average  $E_{NOX}$  in the heating period was about ~~3-12.5~~ times as much as those in the non-heating period. The coal fired heating in Beijing included central heating in urban area and scattered coal combustion in suburb or rural area for the year 2014. We calculated the average  $NO_X$  emission rates of four sectors including industry, power, residential, and transportation from the MEIC within the 6th Ring Rd of Beijing in January, September, and October 2012, and the ratio of each specific  $NO_X$  emission rate in January to the corresponding average value in September and October (Table S1). The  $E_{NOX}$  from the power and residential section were remarkably higher in January than in other two months, and especially  $E_{NOX}$  from the residential was about 5 times more in January than in other months. In general, central heating in urban area are from power plant and residential use the scattered coal combustion in suburb or rural area.

In addition to the seasonal differences, the journey-to-journey variation in estimated  $E_{NOX}$  ~~were-is~~ large even within the same month, mainly due to uncertainties in the calculations of wind speed, ratio of  $NO_2$  and  $NO_X$  concentration, and decay rate of  $NO_X$  from the emission sources to the measured positions under different meteorological conditions. In addition to the  $NO_2$  VCD, wind speed, and wind direction at the sampling points, the estimated  $NO_X$  emission rate is obviously affected by the Leighton ratio of  $NO$  and  $NO_2$  concentration and the lifetime of  $NO_X$  (Valin, et al., 2013). Thus, the estimated  $NO_X$  emission rate could be very large even if the  $NO_2$  VCD was small, such as in the case of September 14~~January 27~~. It should be noted that the low mean wind speed on September 14~~leads January 27 was relatively small and led to higher  $c_T$ , so the  $E_{NOX}$  for this journey is not so low although the  $F_{NO2}$  was very low. In addition, if both  $c_T$  and  $c_L$  are large, high  $E_{NOX}$  can be derived. meanwhile, the ratios of  $NO_X$  and  $NO_2$  were relatively large, so  $E_{NOX}$  on January 27 was large although  $F_{NO2}$  was relatively small. Thus, if  $c_T$  and  $c_L$  are simultaneously larger, higher  $E_{NOX}$  occurs. However, if only one factor is larger and the other is smaller, such as higher  $c_T$  and lower  $c_L$  as on January 18, the morning and afternoon of September 14, and the morning of October 13,  $E_{NOX}$  is lower.~~

### 3.3 Comparisons with MEIC inventory and other estimates

We compared the estimated  $NO_X$  emission with the multi-resolution emission inventory in China (MEIC) released by Tsinghua University for 2012 (MEIC 2012) (Zhang et al., 2009; Zhang et al., 2012). The horizontal resolution of MEIC 2012 is  $0.25^\circ \times 0.25^\circ$ , and five sectors, i.e., agriculture, industry, power, residential~~residents~~, and transportation, are included.

Figure 10 presents the spatial distributions of NO<sub>x</sub> emission rates over Beijing in January, September, and October, 2012, from MEIC. A high NO<sub>x</sub> emission zone was located within the 5th Ring Rd of Beijing, and a low emissions zone occurred in its surroundings in other areas. The NO<sub>x</sub> emissions in January were obviously larger than those in the other two months. ~~The concentrated distribution of NO<sub>x</sub> emission sources within the 5th Ring Rd of Beijing indirectly indicates the applicability of Eq. (1) to estimate the NO<sub>x</sub> emission rates from the car MAX-DOAS measurements on the 6th Ring Rd in this study.~~

Figure 11 shows the ~~journey-to-journey~~ estimated NO<sub>x</sub> emission rates from ~~car~~-Car MAX-DOAS measurements for each selected journey (see Sect. 2.4) in January, September, and October, 2014 (~~denoted as E<sub>NOX</sub>~~), and the corresponding monthly averaged NO<sub>x</sub> emission rates from the MEIC 2012 for the same region within the 6th Ring Rd of Beijing (hereafter expressed as MEIC\_Month). The MEIC\_Month is obviously lower than the estimated E<sub>NOX</sub> in January. While the two emission estimates are very close in September, the MEIC\_Month is slightly smaller than the E<sub>NOX</sub> in October. ~~In most cases, the MEIC\_Month was lower than the estimated E<sub>NOX</sub>, particularly in January.~~ The differences between the estimated E<sub>NOX</sub> and the MEIC\_Month during some journeys were remarkably large. The differences between the E<sub>NOX</sub> and MEIC 2012 during the 10 journeys may be caused by (1) the interannual variations ~~differences~~ in emission inventory, (2) the different timescales of the two emission estimates, (3) the uncertainty of the estimated E<sub>NOX</sub> and MEIC 2012, ~~(4) inconsistency of wind field during the period of measurements, (5) extra transfers from source areas other than urban Beijing, and so on.~~ Firstly, the E<sub>NOX</sub> in this study ~~was~~ is estimated for the year 2014, whereas the ~~MEIC\_Month~~MEIC 2012 was established for the year 2012. Secondly, our results represented only the conditions during a few measurements during daytime, whereas the MIEC 2012 denoted monthly average conditions. Thirdly, the uncertainty of MEIC 2012 is large, particularly in autumn and winter (Li *et al.*, 2017; Meng *et al.*, 2018). There are also large uncertainties in the estimated E<sub>NOX</sub> caused by, e.g., the inconsistency of wind field during a circling journey and the transfer of NO<sub>2</sub> from other source areas than urban Beijing. ~~Fourthly, the emission estimation method used in this study~~ The CIM assumes that the wind field is constant during the ~~period~~ of measurements period and that the wind speed is also sufficiently high ~~that the transport across the encircled area is fast compared to the atmospheric lifetime of the trace gas (Ibrahim *et al.*, 2010).~~ However, the wind field during some journeys (January 27 and October 12,13) ~~might~~ could have changed systematically ~~and been convergent or divergent in some areas of Beijing, as marked as other type of wind field in Table 1.~~ Ibrahim *et al.* (2010) also pointed out that systematic

changes during the ~~period of~~ measurements ~~period~~ can ~~have large impacts on~~ ~~become important to~~ the emission estimate, particularly if measurements with high trace gas VCD are accompanied by strong deviations of the actual wind speed (or direction) from the assumed average values. For example, on the ~~morning-afternoon~~ of January 27, ~~the highest-high~~ NO<sub>2</sub> VCD was measured, and the wind field changed during the measurement journey. In such cases, the systematic changes in wind speed and direction can lead to additional uncertainties in E<sub>NOX</sub>. ~~Moreover Finally,~~ because ~~the~~ southerly wind can bring NO<sub>x</sub> emitted in the south-central regions of Hebei Province to Beijing, the E<sub>NOX</sub> from ~~ear~~-Car MAX-DOAS measurements will be overestimated under south wind conditions, ~~e.g., on January 26.~~

### 3.4 Uncertainty analysis of estimated emissions.

~~We calculated the uncertainty of E<sub>NOX</sub> according to the error transfer formula of relative deviation based on the errors of measured NO<sub>2</sub> VCD, simulated wind speed and direction, and c<sub>L</sub> and c<sub>T</sub>. Figure 11 also shows the uncertainty of E<sub>NOX</sub>, calculated from the errors of measured NO<sub>2</sub> VCD, simulated wind speed, c<sub>L</sub> and c<sub>T</sub> according to the error transfer formula of relative deviation.~~ The standard deviation (STD) of wind speed over a period of time can provide a bound for the related uncertainties of the emission estimate (Ibrahim *et al.*, 2010). Therefore, we first computed the uncertainty of F<sub>NO2</sub> based on the STD of ~~simulated wind speed after correction~~ ~~the corrected wind speed~~ and the measurement error of NO<sub>2</sub> VCD (about ± 10%, Ma *et al.*, 2013a) for each journey. Then, we calculated STD of c<sub>T</sub> according to the first derivative of equation (4) and the ~~monthly~~ STD of c<sub>L</sub> using ~~different NO<sub>x</sub> lifetime and the ratios of NO<sub>x</sub> and NO<sub>2</sub> at sampling position on the 6th Ring Rd of Beijing for each journey.~~ ~~its regional average data within the 6th Ring Rd of Beijing during all journeys in each month. We used the identical STD of c<sub>L</sub> for each journey in the same month to calculate of the uncertainty of E<sub>NOX</sub>.~~ Figure 11 shows the uncertainties of E<sub>NOX</sub> for five journeys and ~~The results showed that the STD ranges of wind speed, c<sub>L</sub> and c<sub>T</sub> were 0.13–1.30 m s<sup>-1</sup>, 0.11–0.37, and 0.17–1.97, respectively. The the uncertainty range of E<sub>NOX</sub> is 2.23 × 10<sup>25</sup> to 9.12 × 10<sup>25</sup> molecules s<sup>-1</sup> (19.52–52.01%).~~ ~~was 16.4–33.2%.~~

~~We also give the spatial variation in the NO<sub>x</sub>/NO<sub>2</sub> ratio and NO<sub>x</sub> lifetime at the entire route for the emission calculation during five journeys (Fig. S7 and S8), and estimate the error contribution of five factors including NO<sub>2</sub> VCD, wind speed, wind direction, the NO<sub>x</sub>/NO<sub>2</sub> ratio, and the NO<sub>x</sub> lifetime to the total uncertainty of E<sub>NOX</sub> (Table 3). In general, there are obvious seasonal and regional difference in the NO<sub>x</sub>/NO<sub>2</sub> ratio and NO<sub>x</sub> lifetime and it is necessary to use specific ratios and lifetime value to estimate~~

the  $E_{\text{NO}_x}$  for each journey. Specifically, the  $\text{NO}_x/\text{NO}_2$  ratio and  $\text{NO}_x$  lifetime are larger in January than in September and October, and they are larger at the southern part of the 6th Ring Rd than at other parts for most journeys. Among error contributions of five factors, the impacts of wind speed and direction are the largest for most journeys except for September 14. For January 26 and 27, error contributions of wind speed to the uncertainty of  $E_{\text{NO}_x}$  are larger than other four factors. For September 14, uncertainty of  $E_{\text{NO}_x}$  is mainly caused by the errors of  $\text{NO}_x$  lifetime and wind direction. For October 12 and 13, error contributions of the  $\text{NO}_x/\text{NO}_2$  ratio are also remarkable. Thus, it is important to obtain the accurate wind vector profiles,  $\text{NO}_x$ ,  $\text{NO}_2$ , and OH concentration data except for  $\text{NO}_2$  VCD to reduce the uncertainty of  $E_{\text{NO}_x}$  estimation using the CIM.

We also calculate the Leighton ratios,  $L_r$ , to assess impacts of VOCs on the  $\text{NO}_x$  lifetime. The  $L_r$  during five journeys is 0.85, 0.80, 1.04, 1.19, and 1.33 on January 26 and 27, September 14, October 12 and 13, respectively. Results show that the  $\text{NO}_x$  lifetime for the three journeys on September and October are affected by VOCs and lead to extra errors of  $E_{\text{NO}_x}$ . While VOCs can't cause the deviation in the  $\text{NO}_x$  lifetime and estimation of the  $E_{\text{NO}_x}$  in January.

#### 4. Conclusions

We carried out 19 city-circle-around ~~ear~~-Car MAX-DOAS experiments on the 6th Ring Rd of Beijing in January, September, and October, 2014. The VCD of  $\text{NO}_2$  was retrieved and the temporal and spatial distributions were investigated. Then the  $\text{NO}_x$  emission rates in urban Beijing were estimated using the measured  $\text{NO}_2$  VCD together with the refined wind fields,  $\text{NO}_2$  to  $\text{NO}_x$  ratios, and  $\text{NO}_2$  lifetimes simulated by the LAPS-WRF-CMAQ model system, and the results were compared to the emission rates from the MEIC inventory 2012.

The ~~mean, maximum, and minimum~~  $\text{NO}_2$  VCD values averaged for each experimental journey during the sampling periods in January were all larger than those in the other two months, mainly due to higher emissions in winter. The ~~measured mean~~  $\text{NO}_2$  VCD was typically larger at the southern parts of the 6th Ring Road than at the northern parts because weak south wind resulted in the transport and accumulation of  $\text{NO}_2$  from southern areas in Hebei Province and strong north wind suppressed the transport of  $\text{NO}_2$  from the southern area. Such inhomogeneous distributions of tropospheric  $\text{NO}_2$  VCD bring a challenge for the validation of satellite products for Beijing as well as other megacities.

The journey-to-journey variation in estimated  $E_{\text{NO}_x}$  were large, even within the same month, mainly

due to uncertainties in the calculation of wind speed, the ratio of NO<sub>2</sub> and NO<sub>x</sub> concentration, and the decay rate of NO<sub>x</sub> from the emission sources to the measured positions under different meteorological conditions. ~~The ranges of E<sub>NOX</sub> during the heating and non-heating periods were  $28.7 \times 10^{25}$  to  $60.0 \times 10^{25}$  molecules s<sup>-1</sup> and  $7.7 \times 10^{25}$  to  $24.8 \times 10^{25}$  molecules s<sup>-1</sup>, respectively.~~ The average E<sub>NOX</sub> values in the heating and non-heating periods ~~were~~ are estimated to be  $26.94 \pm 6.1443.0 \times 10^{25}$  molecules s<sup>-1</sup> and  $10.99 \pm 1.23 13.9 \times 10^{25}$  molecules s<sup>-1</sup>, respectively, ~~with an-~~ The uncertainty range of E<sub>NOX</sub> ~~was~~ 19.52–52.01%16.4–33.2%. The monthly emission rates in the area within the 6th Ring Rd of Beijing from MEIC 2012 ~~are were~~ lower than the estimated E<sub>NOX</sub>, particularly in January. The differences between the E<sub>NOX</sub> and the monthly emission rates from MEIC 2012 ~~may-can~~ be attributed attributable to the interannual differences in the emissions inventory, the different timescales and uncertainties of two kinds of inventory, ~~inconsistencies of wind field during the period of measurements, and extra transfers from source areas other than urban Beijing.~~

Our results showed that ~~ear-Car~~ MAX-DOAS measurements can be used effectively for dynamic monitoring and updating of the NO<sub>x</sub> emissions from megacities such as Beijing. To estimate ~~the~~ E<sub>NOX</sub> by ~~ear-Car~~ MAX-DOAS accurately in Beijing and other similar megacities, appropriate meteorological conditions, such as smaller fluctuations of the wind field, relatively larger wind speed, and suitable wind direction, need to be selected to avoid the impact of extra transfers of large emission sources from surrounding areas. In addition to the NO<sub>2</sub> VCD, simultaneous observations of wind speed, wind direction, and surface NO and NO<sub>2</sub> concentrations are recommended to reduce the uncertainties of ~~E<sub>NOX</sub> c<sub>r</sub> and c<sub>t</sub>.~~

*Data availability.* The NCEP-FNL reanalysis and ECMWF are publicly available at <http://rda.ucar.edu/datasets/ds083.2/> and <https://www.ecmwf.int/en/forecasts/datasets>, respectively. The NO<sub>2</sub> - measurements and meteorological observations including wind speed and wind direction data are available at <http://113.108.142.147:20035/emcpublish> and <http://data.cma.cn/>, respectively. The tropospheric NO<sub>2</sub> VCD data derived from this study are available on the request.

*Author contributions.* JM and XC designed the research. JM, JJ, JG, MQ, QX, and PY contributed to the measurements, and JM performed the spectral analysis and retrieval. XC and JP designed the model experiment and performed the model simulations. XC, YL, JP, and XM contributed to the data processing and analyses. XC and JM analyzed the results and wrote the paper with inputs from all authors.

*Competing interests.* The authors declare that they have no conflicts of interest.

590 *Acknowledgments.* This work was supported jointly by the National Natural Science Foundation of China  
(91644223), the National Research Program for Key Issues in Air Pollution Control (DQGG0104), and  
the Scientific and Technological Development Funds from the Chinese Academy of Meteorological  
Sciences (2018KJ042). The authors acknowledge Tsinghua University for providing the emissions  
inventory and the China National Environmental Monitoring Centre for providing surface ~~PM<sub>2.5</sub>~~NO<sub>2</sub>  
595 observation data.

## References

Albers, S. C., McGinley, J. A., Birkenheuer, D., and Smart, J. R.: The local analysis and prediction system  
(LAPS): Analyses of clouds, precipitation, and temperature, *Wea. Forecasting*, 11, 273-287, 1996.

Brinksma, E. J., Pinardi, G., Volten, H., Braak, R., Richter, A., Schoenhardt, A., van Roozendaal, M.,  
600 Fayt, C., Hermans, C., Dirksen, R. J., Vlemmix, T., Berkhout, A. J. C., Swart, D. P. J., Oetjen, H.,  
Wittrock, F., Wagner, T., Ibrahim, O. W., de Leeuw, G., Moerman, M., Curier, R. L., Celarier, E. A.,  
Cede, A., Knap, W. H., Veefkind, J. P., Eskes, H. J., Allaart, M., Rothe, R., Piters, A. J. M. and Levelt,  
P. F.: The 2005 and 2006 DANDELIONS NO<sub>2</sub> and aerosol intercomparison campaigns, *J. Geophys.*  
*Res.-Atmospheres*, 113(D16), D16S46, doi:10.1029/2007JD008808, 2008.

605 Burrows, J. P., Richter, A., Dehn, A., Deters, B., Himmelmann, S., Voigt, S., and Orphal, J.: Atmospheric  
remote sensing reference data from GOME-2. temperature-dependent absorption cross-sections of O<sub>3</sub>  
in the 231-794 nm range, *J. Quant. Spectrosc. Ra.*, 61, 509-517, 1999.

Cao, C., Jiang, W., Wang, B., Fang, J., Lang, J., Tian, G., Jiang, J., and Zhu, T. F.: Inhalable  
microorganisms in Beijing's PM<sub>2.5</sub> and PM<sub>10</sub> pollutants during a severe smog event, *Environ Sci*  
610 *Technol*, 48, 1499-1507, 10.1021/es4048472, 2014.

Cheng, X., Sun, Z., Li, D., Xu, X., Jia, M., and Cheng, S.: Short-term aerosol radiative effects and their  
regional difference during heavy haze episodes in January 2013 in China, *Atmospheric Environment*,  
165, 248-263, 10.1016/j.atmosenv.2017.06.040, 2017.

Davis, Z. Y. W., Baray, S., McLinden, C. A., Khanbabakhani, A., Fujs, W., Csukat, C., Debosz, J. and

- 615 McLaren, R.: Estimation of NO<sub>x</sub> and SO<sub>2</sub> emissions from Sarnia, Ontario, using a mobile MAX-DOAS (Multi-AXis Differential Optical Absorption Spectroscopy) and a NO<sub>x</sub> analyzer, *Atmospheric Chem. Phys.*, 19(22), 13871–13889, doi:<https://doi.org/10.5194/acp-19-13871-2019>, 2019.
- Dennis, R., Byun, D., and Novak, J.: The next generation of integrated air quality modeling: EPA's Models-3, *Atmos. Environ.*, 30, 1925–1938, 1996.
- 620 [Dickerson, R. R., Stedman, D. H., and Delany, A. C.: Direct measurements of ozone and nitrogen dioxide photolysis rates in the troposphere, \*Journal of Geophysical Research\*, 87, 10.1029/JC087iC07p04933, 1982.](#)
- Fayt, C., and Van Roozendaal, M.: WinDOAS 2.1 software user manual, IASB/BIRA Uccle, Belgium, 2011.
- 625 Greenblatt, G. D., Orlando, J. J., Burkholder, J. B., and Ravishankara, A. R.: Absorption measurements of oxygen between 330 and 1140 nm, *J. Geophys. Res.*, 95, 18577–18582, 10.1029/JD095iD11p18577, 1990.
- [Hönninger, G. and Platt, U.: Observations of BrO and its vertical distribution during surface ozone depletion at Alert, \*Atmos. Environ.\*, 36, 2481–2489, \[https://doi.org/10.1016/S1352-2310\\(02\\)00104-8\]\(https://doi.org/10.1016/S1352-2310\(02\)00104-8\), 2002.](#)
- 630 Hönninger, G., von Friedeburg, C., and Platt, U.: Multi axis differential optical absorption spectroscopy (MAX-DOAS), *Atmos. Chem. Phys.*, 4, 231–254, 10.5194/acp-4-231-2004, 2004.
- Hao, J., Tian, H., and Lu, Y.: Emission inventories of NO<sub>x</sub> from commercial energy consumption in China, 1995–1998, *Environmental Science and Technology*, 36, 552–560, 2002.
- 635 He, H., Wang, X. M., Wang, Y. S., Wang, Z. F., Liu, J. G., and Chen, Y. F.: Formation Mechanism and Control Strategies of Haze in China, *Bull. Chin. Acad. Sci.*, 28, 344–352, 2013.
- Hendrick, F., Müller, J. F., Clémer, K., Wang, P., De Mazière, M., Fayt, C., Gielen, C., Hermans, C., Ma, J. Z., Pinardi, G., Stavrou, T., Vlemmix, T., and Van Roozendaal, M.: Four years of ground-based MAX-DOAS observations of HONO and NO<sub>2</sub> in the Beijing area, *Atmospheric Chemistry and*
- 640 *Physics*, 14, 765–781, 10.5194/acp-14-765-2014, 2014.
- Huang, R. J., Zhang, Y., Bozzetti, C., Ho, K. F., Cao, J. J., Han, Y., Daellenbach, K. R., Slowik, J. G., Platt, S. M., Canonaco, F., Zotter, P., Wolf, R., Pieber, S. M., Bruns, E. A., Crippa, M., Ciarelli, G., Piazzalunga, A., Schwikowski, M., Abbaszade, G., Schnelle-Kreis, J., Zimmermann, R., An, Z., Szidat, S., Baltensperger, U., El Haddad, I., and Prevot, A. S.: High secondary aerosol contribution to
- 645 particulate pollution during haze events in China, *Nature*, 514, 218–222, 10.1038/nature13774, 2014.
- Ibrahim, O., Shaiganfar, R., Sinreich, R., Stein, T., Platt, U., and Wagner, T.: Car MAX-DOAS



- measurements around entire cities: quantification of NO<sub>x</sub> emissions from the cities of Mannheim and Ludwigshafen (Germany), *Atmos. Meas. Tech.*, 3, 709-721, 10.5194/amt-3-709-2010, 2010.
- Irie, H., Kanaya, Y., Akimoto, H., Z., W., Gleason, J. F., and Bucsela, E. J.: Validation of OMI  
650 tropospheric NO<sub>2</sub> column data using MAX-DOAS measurements deep inside the North China Plain in June 2006 Mount Tai Experiment 2006, *Atmos. Chem. Phys.*, 8, 6577-6586, 2008.
- Jaegle', L., Steinberger, L., Martin, R. V., and Chance, K.: Global partitioning of NO<sub>x</sub> sources using satellite observations: relative roles of fossil fuel combustion, biomass burning and soil emissions, *The Royal Society of Chemistry*, 130, 407-423, 2005.
- 655 Jin, J., Ma, J., Lin, W., Zhao, H., Shaiganfar, R., Beirle, S., and Wagner, T.: MAX-DOAS measurements and satellite validation of tropospheric NO<sub>2</sub> and SO<sub>2</sub> vertical column densities at a rural site of North China, *Atmospheric Environment*, 133, 12-25, <http://dx.doi.org/10.1016/j.atmosenv.2016.03.031>, 2016.
- Johansson, M., Galle, B., Yu, T., Tang, L., Chen, D., Li, H., Li, J. X., and Zhang, Y.: Quantification of  
660 total emission of air pollutants from Beijing using mobile mini-DOAS, *Atmospheric Environment*, 42, 6926-6933, <http://dx.doi.org/10.1016/j.atmosenv.2008.05.025>, 2008.
- Johansson, M., Rivera, C., de Foy, B., Lei, W., Song, J., Zhang, Y., Galle, B., and Molina, L.: Mobile mini-DOAS measurement of the outflow of NO<sub>2</sub> and HCHO from Mexico City, *Atmos. Chem. Phys.*, 9, 5647-5653, 10.5194/acp-9-5647-2009, 2009.
- 665 Konovalov, I. B., Beekmann, M., Richter, A., and Burrows, J. P.: Inverse modeling of the spatial distribution of NO<sub>x</sub> emissions on a continental scale using satellite data, *Atmospheric Chemistry and Physics*, 6, 1747-1770, 2006.
- Kraus, S.: DOASIS, DOAS for Windows software [CD-ROM], in: Proceedings of the 1st International DOAS-Workshop, Heidelberg, Germany, 13-14 September 2001, 2001a.
- 670 Kraus, S.: DOASIS, DOAS for Windows software [CD-ROM], in: Proceedings of the 1st International DOAS-Workshop, Heidelberg, Germany, 13-14 September 2001, 2001b.
- Li, M., Liu, H., Geng, G., Hong, C., Liu, F., Song, Y., Tong, D., Zheng, B., Cui, H., Man, H., Zhang, Q., and He, K.: Anthropogenic emission inventories in China: a review, *National Science Review*, 4, 834-866, 10.1093/nsr/nwx150, 2017.
- 675 Li, X., Brauers, T., Hofzumahaus, A., Lu, K., Li, Y., Shao, M., Wagner, T., and Wahner, A.: MAX-DOAS measurements of NO<sub>2</sub>, HCHO and CHOCHO at a rural site in Southern China, *Atmospheric*

Chemistry and Physics, 13, 2133-2151, 2013.

Liao, L., Lou, S. J., Fu, Y., Chang, W. J., and Liao, H.: Radiative forcing of aerosols and its impact on surface air temperature on the synoptic scale in eastern China, *Chin. J. Atmos. Sci. (Chin. Ver.)*, 39, 68-82, 2015.

Lin, J. T., Liu, Z., Zhang, Q., Liu, H., Mao, J., and Zhuang, G.: Modeling uncertainties for tropospheric nitrogen dioxide columns affecting satellite-based inverse modeling of nitrogen oxides emissions, *Atmospheric Chemistry and Physics*, 12, 12255-12275, 10.5194/acp-12-12255-2012, 2012.

Ma, J., and Van Aardenne, J. A.: Impact of different emission inventories on simulated tropospheric ozone over China: a regional chemical transport model evaluation, *Atmos. Chem. Phys.*, 4, 877-887, 2004.

Ma, J. Z., Wang, W., Chen, Y., Liu, H. J., Yan, P., Ding, G. A., Wang, M. L., Sun, J., and Lelieveld, J.: The IPAC-NC field campaign: a pollution and oxidization pool in the lower atmosphere over Huabei, China, *Atmos. Chem. Phys.*, 12, 3883-3908, 10.5194/acp-12-3883-2012, 2012.

Ma, J., Wang, W., Liu, H., Chen, Y., Xu, X., and Lelieveld, J.: Pollution plumes observed by aircraft over North China during the IPAC-NC field campaign, *Chinese Science Bulletin*, 58, 4329-4336, 10.1007/s11434-013-5978-9, 2013.

Ma, J. Z., Beirle, S., Jin, J. L., Shaiganfar, R., Yan, P., and Wagner, T.: Tropospheric NO<sub>2</sub> vertical column densities over Beijing: results of the first three years of ground-based MAX-DOAS measurements (2008&ndash;2011) and satellite validation, *Atmospheric Chemistry and Physics*, 13, 1547-1567, 10.5194/acp-13-1547-2013, 2013a.

Martin, R. V.: An improved retrieval of tropospheric nitrogen dioxide from GOME, *Journal of Geophysical Research*, 107, 10.1029/2001jd001027, 2002.

McGinley, J. A., Albers, S., and Stamus, P.: Validation of a composite convective index as defined by a real-time local analysis system, *Wea.Forecasting*, 6, 337-356, 1991.

Meng, K., Xu, X., Cheng, X., Xu, X., Qu, X., Zhu, W., Ma, C., Yang, Y., and Zhao, Y.: Spatio-temporal variations in SO<sub>2</sub> and NO<sub>2</sub> emissions caused by heating over the Beijing-Tianjin-Hebei Region constrained by an adaptive nudging method with OMI data, *The Science of the total environment*, 642, 543-552, 10.1016/j.scitotenv.2018.06.021, 2018.

Michalakes, J., Dudhia, J., Gill, D., Henderson, T., Klemp, J., Skamarock, W., and Wang, W.: The weather research and forecast model: software architecture and performance, the 11th ECMWF Workshop on the Use of High Performance Computing In Meteorology, George Mozdzyński, 2004.

- Otte, T. L., and Pleim, J. E.: The Meteorology-Chemistry Interface Processor (MCIP) for the CMAQ modeling system: updates through MCIPv3.4.1, *Geosci. Model Dev.*, 3, 243-256, 2010.
- Platt, U.: Differential optical absorption spectroscopy (DOAS), in: *Air Monitoring by Spectroscopic Techniques*, edited by: Sigrist, M. W., Chemical Analysis Series, 127, John Wiley, New York, 27–84, 1994.
- Platt, U., and Stutz, J.: *Differential Optical Absorption Spectroscopy Principles and Applications*, Physics of Earth and Space Environments, Springer, Heidelberg, 2008.
- Shaiganfar, R., Beirle, S., Sharma, M., Chauhan, A., Singh, R. P., and Wagner, T.: Estimation of NO<sub>x</sub> emissions from Delhi using Car MAX-DOAS observations and comparison with OMI satellite data, *Atmos. Chem. Phys.*, 11, 10871-10887, 10.5194/acp-11-10871-2011, 2011.
- Shaiganfar, R., Beirle, S., van der Gon, H. D., Jonkers, S., Kuenen, J., Petetin, H., Zhang, Q., Beekmann, M. and Wagner, T.: Estimation of the Paris NO<sub>x</sub> emissions from mobile MAX-DOAS observations and CHIMERE model simulations during the MEGAPOLI campaign using the closed integral method, *Atmospheric Chem. Phys.*, 17(12), 7853–7890, doi:10.5194/acp-17-7853-2017, 2017.
- Streets, D. G., Canty, T., Carmichael, G. R., de Foy, B., Dickerson, R. R., Duncan, B. N., Edwards, D. P., Haynes, J. A., Henze, D. K., Houyoux, M. R., Jacob, D. J., Krotkov, N. A., Lamsal, L. N., Liu, Y., Lu, Z., Martin, R. V., Pfister, G. G., Pinder, R. W., Salawitch, R. J., and Wecht, K. J.: Emissions estimation from satellite retrievals: A review of current capability, *Atmospheric Environment*, 77, 1011-1042, 10.1016/j.atmosenv.2013.05.051, 2013.
- Tan, T., Hu, M., Li, M., Guo, Q., Wu, Y., Fang, X., Gu, F., Wang, Y., and Wu, Z.: New insight into PM<sub>2.5</sub> pollution patterns in Beijing based on one-year measurement of chemical compositions, *The Science of the total environment*, 621, 734-743, 10.1016/j.scitotenv.2017.11.208, 2018.
- UNC: SMOKE v3.6 user's manual, Chapel Hill: The institute for the Environmen, 2014.
- Vandaele, A. C., Hermans, C., Simon, P. C., Carleer, M., Colin, R., Fally, S., Mérienne, M. F., Jenouvrier, A., and Coquart, B.: Measurements of the NO<sub>2</sub> absorption cross-section from 42 000 cm<sup>-1</sup> to 10 000 cm<sup>-1</sup> (238–1000 nm) at 220 K and 294 K, *J. Quant. Spectrosc. Ra.*, 59, 171-184, 1998.
- Valin, L. C., Russell, A. R. and Cohen, R. C.: Variations of OH radical in an urban plume inferred from NO<sub>2</sub> column measurements, *Geophys. Res. Lett.*, 40(9), 1856–1860, doi:10.1002/grl.50267, 2013.
- Vlemmix, T., Piters, A., Stammes, P., Wang, P., and Levelt, P.: Retrieval of tropospheric NO<sub>2</sub> using the MAX-DOAS method combined with relative intensity measurements for aerosol correction,

Atmospheric Measurement Techniques, 3, 1287-1305, 2010.

Wagner, T., Dix, B., Friedeburg, C. v., Frieß, U., Sanghavi, S., Sinreich, R., and Platt, U.: MAX-DOAS  
O<sub>4</sub> measurements: A new technique to derive information on atmospheric aerosols -- Principles and  
information content, J. Geophys. Res., 109, D22205, 10.1029/2004jd004904, 2004.

Wagner, T., Ibrahim, O., Shaiganfar, R., and Platt, U.: Mobile MAX-DOAS observations of tropospheric  
trace gases, Atmos. Meas. Tech., 3, 129-140, 2010a.

Wagner, T., Ibrahim, O., Shaiganfar, R., and Platt, U.: Mobile MAX-DOAS observations of tropospheric  
trace gases, Atmos. Meas. Tech., 3, 129-140, 10.5194/amt-3-129-2010, 2010b.

Wagner, T., Beirle, S., Brauers, T., Deutschmann, T., Frieß, U., Hak, C., Halla, J. D., Heue, K. P.,  
Junkermann, W., Li, X., Platt, U., and Pundt-Gruber, I.: Inversion of tropospheric profiles of aerosol  
extinction and HCHO and NO<sub>2</sub>; mixing ratios from MAX-DOAS observations in Milano during the  
summer of 2003 and comparison with independent data sets, Atmospheric Measurement Techniques,  
4, 2685-2715, 10.5194/amt-4-2685-2011, 2011.

Wang, S., Zhou, B., Wang, Z., Yang, S., Hao, N., Valks, P., Trautmann, T., and Chen, L.: Remote sensing  
of NO<sub>2</sub> emission from the central urban area of Shanghai (China) using the mobile DOAS technique,  
Journal of Geophysical Research: Atmospheres, 117, D13305, 10.1029/2011jd016983, 2012.

Wang, Y., McElroy, M. B., Martin, R. V., Streets, D. G., Zhang, Q., and Fu, T.-M.: Seasonal variability  
of NO<sub>x</sub> emissions over east China constrained by satellite observations: Implications for combustion  
and microbial sources, Journal of Geophysical Research, 112, 10.1029/2006jd007538, 2007.

Wittrock, F., Oetjen, H., Richter, A., Fietkau, S., Medeke, T., Rozanov, A., and Burrows, J.: MAX-DOAS  
measurements of atmospheric trace gases in Ny-Ålesund-Radiative transfer studies and their  
application, Atmos. Chem. Phys., 4, 955-966, 2004.

Wu, F., Xie, P., Li, A., Mou, F., Chen, H., Zhu, Y., Zhu, T., Liu, J., and Liu, W.: Investigations of temporal  
and spatial distribution of precursors SO<sub>2</sub> and NO<sub>2</sub>~~&lt;sub>2</sub>&lt;/del> and  
~~NO<sub>2</sub>~~~~&lt;sub>2</sub>&lt;/del>~~; vertical columns in the North China Plain using mobile DOAS,  
Atmospheric Chemistry and Physics, 18, 1535-1554, 10.5194/acp-18-1535-2018, 2018.~~

Zhang, Q., Streets, D. G., He, K., Wang, Y., Richter, A., Burrows, J. P., Uno, I., Jang, C. J., Chen, D., Yao,  
Z., and Lei, Y.: NO<sub>x</sub> emission trends for China, 1995–2004: The view from the ground and the view  
from space, Journal of Geophysical Research, 112, 10.1029/2007jd008684, 2007.

Zhang, Q., Streets, D. G., Carmichael, G. R., He, K. B., Huo, H., Kannari, A., Klimont, Z., Park, I. S.,  
Reddy, S., Fu, J. S., Chen, D., Duan, L., Lei, Y., Wang, L. T., and Yao, Z. L.: Asian emissions in 2006

for the NASA INTEx-B mission, *Atmos. Chem. Phys.*, 9, 5131-5153, 2009.

Zhang, Q., Geng, G., Wang, S., Richter, A., and He, K.: Satellite remote sensing of changes in NO<sub>x</sub>

770 emissions over China during 1996–2010, *Chinese Science Bulletin*, 57, 2857-2864, 10.1007/s11434-012-5015-4, 2012.

Zhang, X. Y., Sun, J. Y., Wang, Y. Q., Li, W. J., Zhang, Q., Wang, W. G., Quan, J. N., Cao, G. L., Wang, J. Z., Yang, Y. Q., and Zhang, Y. M.: Factors contributing to haze and fog in China, *Chin. Sci. Bull. (Chin. Ver.)*, 58, 1178-1187, 2013.

775 Zhao, B., Wang, P., Ma, J. Z., Zhu, S., Pozzer, A., and Li, W.: A high-resolution emission inventory of primary pollutants for the Huabei region, China, *Atmospheric Chemistry and Physics*, 12, 481-501, 10.5194/acp-12-481-2012, 2012.

Zyrichidou, I., Koukouli, M. E., Balis, D., Markakis, K., Poupkou, A., Katragkou, E., Kioutsioukis, I., Melas, D., Boersma, K. F., and van Roozendaal, M.: Identification of surface NO<sub>x</sub> emission sources  
780 on a regional scale using OMI NO<sub>2</sub>, *Atmospheric Environment*, 101, 82-93, 10.1016/j.atmosenv.2014.11.023, 2015.

785

790

795

Table 1. Sampling periods of the ~~ear~~-Car MAX-DOAS experiment and corresponding meteorological conditions over Beijing in January, September, and October, 2014.

Journey	Date	Time (BJT)	Wind speed (m/s)	Type of wind field*	Total cloud fraction	PBL Height (m)
1**	2014/1/18	10:48-13:09	2	<del>St</del> Θ	0	564
2	2014/1/19	13:31-15:40	1	O	7	167
3**	2014/1/21	13:15-15:32	3	S	0	163
4	2014/1/23	10:39-12:25	3	O	7	187
5	2014/1/23	13:07-15:12	2	O	7	163
6**	2014/1/24	10:42-12:03	2	N	8	39
7**	2014/1/24	13:03-15:09	3	N	8	39
8**	2014/1/26	10:21-12:13	5	S	5	341
9**	2014/1/27	09:11-11:38	2	<del>St</del> Θ	7	75
10**	2014/1/27	13:30-15:28	2	O	0	178
11**	2014/9/14	09:40-12:52	4	N	10	173
12**	2014/9/14	15:02-17:17	2	N	10	226
13**	2014/9/17	09:07-11:42	2	<del>St</del> Θ	7	173
14**	2014/9/19	09:09-11:50	2	S	3	178
15	2014/10/9	13:04-14:44	1	<del>St</del> S	7	43
16**	2014/10/10	09:52-12:28	2	S	7	663
17**	2014/10/12	14:02-16:42	3	N	7	167
18**	2014/10/13	09:12-11:59	3	<del>N</del> Θ	0	186
19**	2014/10/13	13:11-16:27	3	O	0	130

\*Four types of wind filed are South (S), North (N), Other (O), and Static (St).

\*\*The data are preliminarily selected to estimate the NO<sub>x</sub> emissions.

\*Three types of wind filed are South (S), North (N) and Other (O).

\*\*The data from ten circling journeys are used to estimate the NO<sub>x</sub> emission.

Table 2. Overview of the problems for the six circling journeys.

<u>Date</u>	<u>Time (BJT)</u>	<u>Large wind variability</u> *	<u>Large lifetime correction</u> *	<u>Gap/route close to the centre</u> *	<u>Small difference between influx and outflux</u> *	<u>Multiple problems</u> **
<u>2014/1/26***</u>	<u>10:21-12:13</u>	<u>N</u>	<u>N</u>	<u>N</u>	<u>Y</u>	<u>N</u>
<u>2014/1/27***</u>	<u>13:30-15:28</u>	<u>Y</u>	<u>N</u>	<u>N</u>	<u>N</u>	<u>N</u>
<u>2014/9/14</u>	<u>09:40-12:52</u>	<u>Y</u>	<u>Y</u>	<u>Y</u>	<u>N</u>	<u>Y</u>
<u>2014/9/14***</u>	<u>15:02-17:17</u>	<u>N</u>	<u>Y</u>	<u>N</u>	<u>N</u>	<u>N</u>
<u>2014/10/12***</u>	<u>14:02-16:42</u>	<u>Y</u>	<u>Y</u>	<u>N</u>	<u>N</u>	<u>Y</u>
<u>2014/10/13***</u>	<u>09:12-11:59</u>	<u>Y</u>	<u>Y</u>	<u>N</u>	<u>N</u>	<u>Y</u>

\*Whether the condition meets the criteria of Shaiganfar et al. (2017) or not, Y and N denote Yes and No respectively.

\*\* Multiple problems mean whether more than two conditions can meet the criteria or not.

\*\*\* The data of five circling journeys are ultimately used to estimate the NO<sub>x</sub> emission.

Table 3. Error contributions (%) of multiple factors to the uncertainties in estimated E<sub>NO<sub>x</sub></sub> during five circling journeys.

<u>Factors</u>	<u>Jan. 26, AM</u>	<u>Jan. 27, PM</u>	<u>Sep. 14, PM</u>	<u>Oct. 12, PM</u>	<u>Oct. 13, AM</u>
<u>VCD<sub>geo</sub></u>	<u>10</u>	<u>10</u>	<u>10</u>	<u>10</u>	<u>10</u>
<u>Wind speed</u>	<u>27.02</u>	<u>26.83</u>	<u>7.97</u>	<u>33.10</u>	<u>3.68</u>
<u>Wind direction</u>	<u>10.97</u>	<u>16.50</u>	<u>20.54</u>	<u>33.78</u>	<u>38.37</u>
<u>NO<sub>x</sub>/NO<sub>2</sub> ratio</u>	<u>12.21</u>	<u>13.46</u>	<u>7.82</u>	<u>29.33</u>	<u>29.48</u>
<u>Lifetime</u>	<u>3.63</u>	<u>7.67</u>	<u>48.60</u>	<u>15.22</u>	<u>19.02</u>

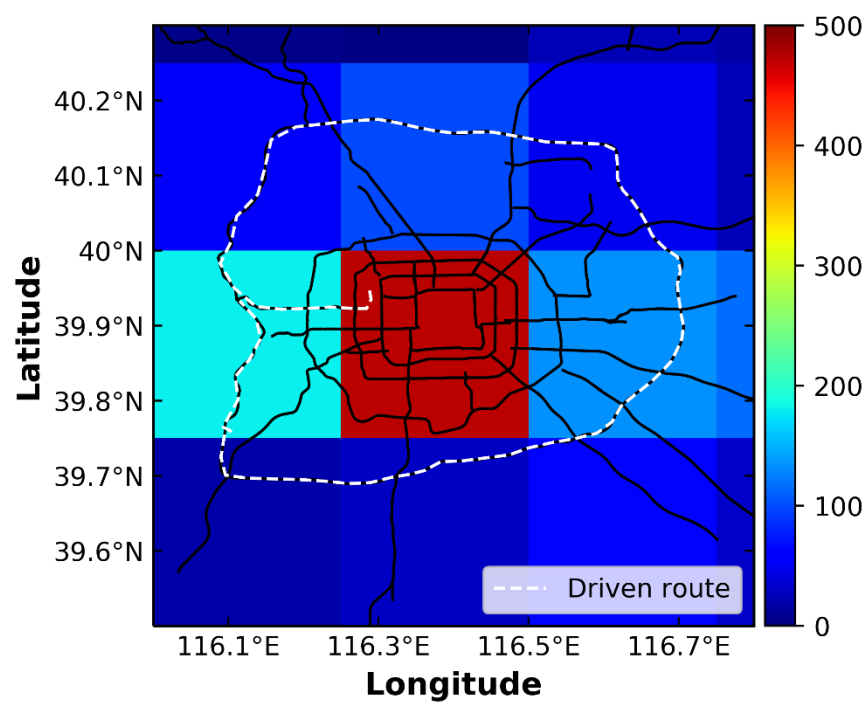


**Fig. 1** Driving routes (white dash red-line) of the car MAX-DOAS experiment on the 6th Ring Rd of Beijing and distribution of yearly averaged NO<sub>x</sub> emission rate (mole km<sup>-2</sup> h<sup>-1</sup>) from the MEIC for the year 2012.



865

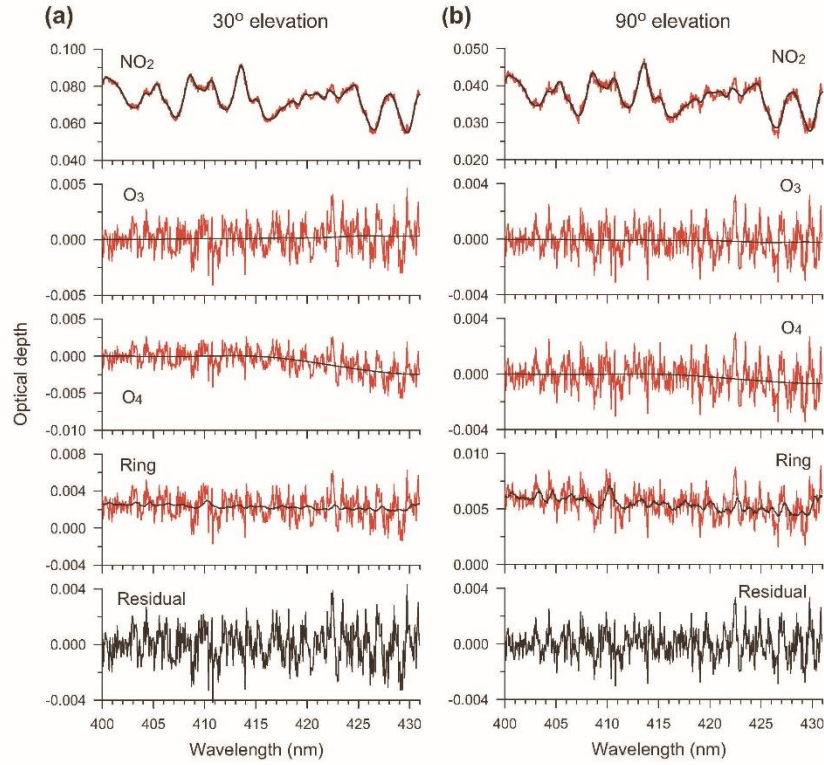


**Fig. 2** Examples of the NO<sub>2</sub> retrieval from two successive spectra measured **(a)** at a 30° elevation angle (with NO<sub>2</sub> differential slant column density (DSCD) of  $1.23 \times 10^{17}$  molecules cm<sup>-2</sup>) and **(b)** at a 90° elevation angle (with NO<sub>2</sub> DSCD of  $6.22 \times 10^{16}$  molecules cm<sup>-2</sup>) on January 18, 2014, at around 11:40 BJT.

870

875

880

885

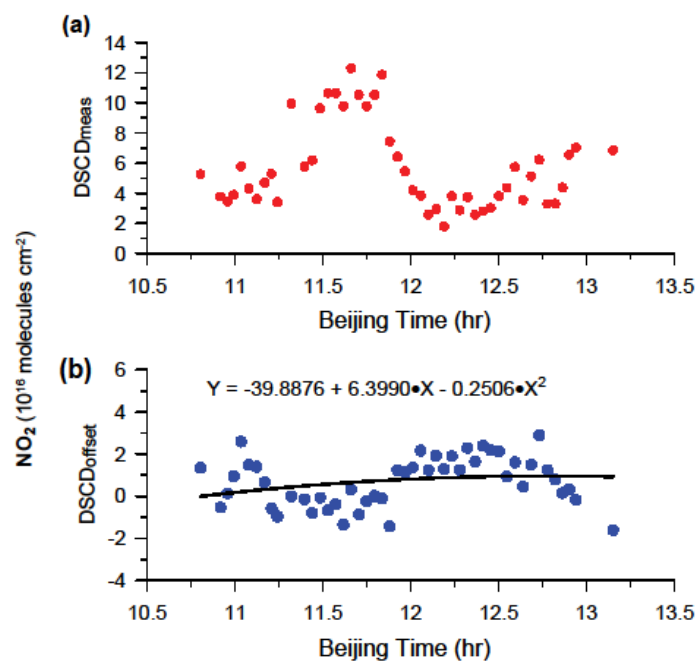


**Fig. 3** Time series of the NO<sub>2</sub> (a) DSCD<sub>means</sub> (red dots) and (b) DSCD<sub>offset</sub> (black dots) (units of 10<sup>16</sup> molecules cm<sup>-2</sup>) for the 30° elevation angle of each sequence on January 18, 2014. The black curve represents a second-order polynomial fit from individual DSCD<sub>offset</sub> data points.

890

895

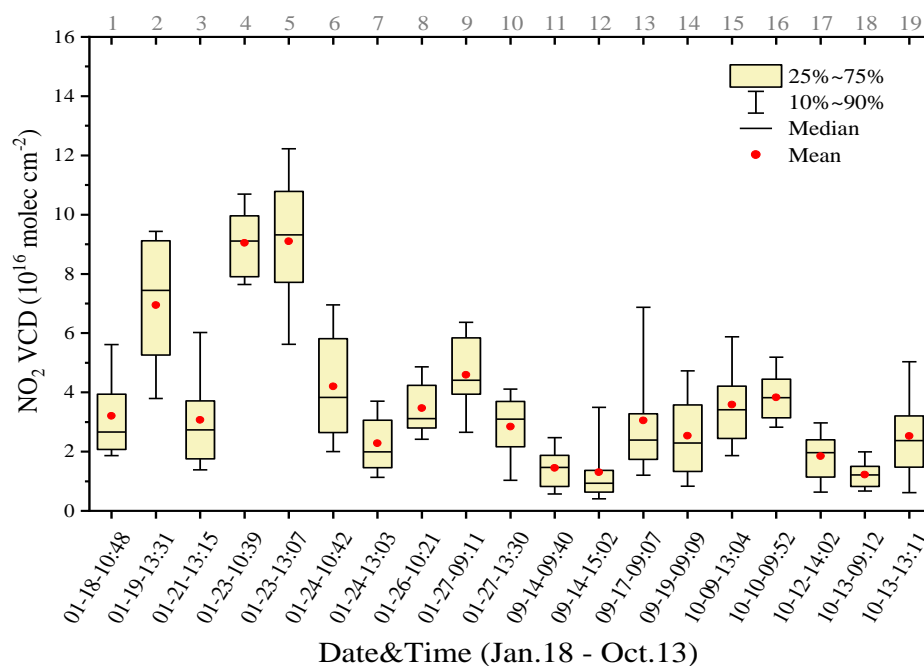


**Fig. 4** Time series of the tropospheric NO<sub>2</sub> vertical column density (VCD) for 19 circling journeys on the Sixth Ring Road of Beijing in January, September, and October, 2014. Lower (upper) error bars and yellow boxes are the 10th (90th) and 25th (75th) percentiles of the data of each journey, respectively. Hyphens inside the boxes are the medians, and red circles are the mean values. The numbers of each journey are labeled at the top axis. See Table 1 for detailed information about each journey.

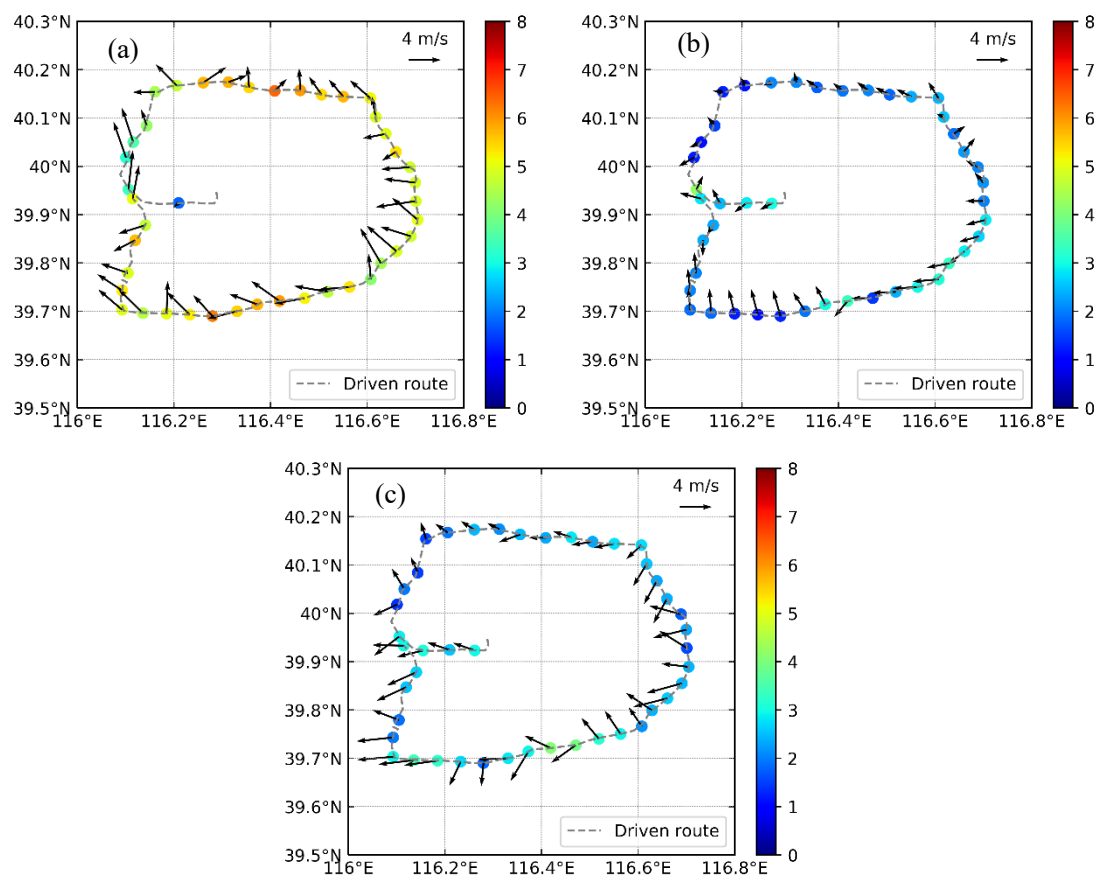


**Fig. 5** Distributions of the monthly averaged average-NO<sub>2</sub> VCD ( $10^{16}$  molecules cm<sup>-2</sup>) on the 6th Ring Rd of Beijing in (a) January, (b) September, and (c) October, 2014.

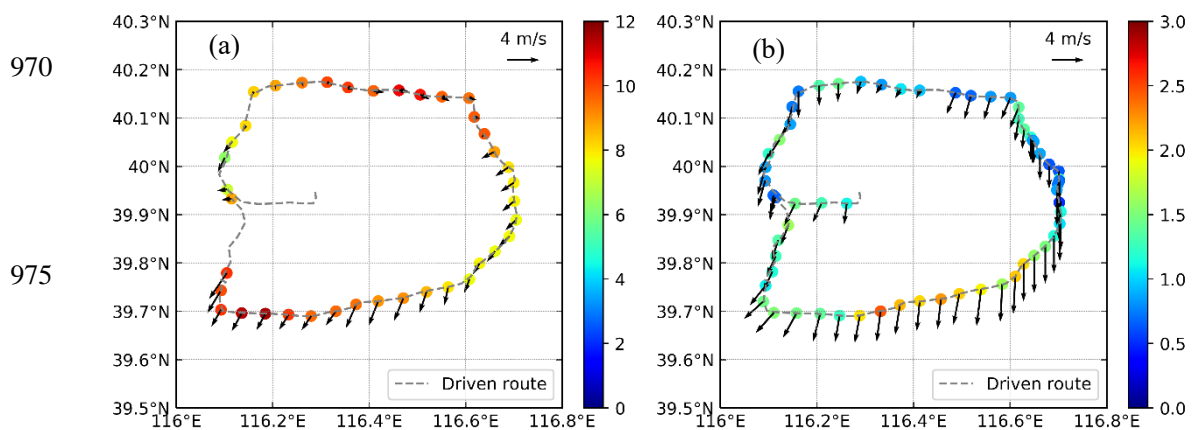


**Fig. 6** Distributions of the maximum and minimum NO<sub>2</sub> VCD ( $10^{16}$  molecules cm<sup>-2</sup>) on the 6th Ring Rd of Beijing on the morning of **(a)** January 23 and **(b)** October 13, 2014.

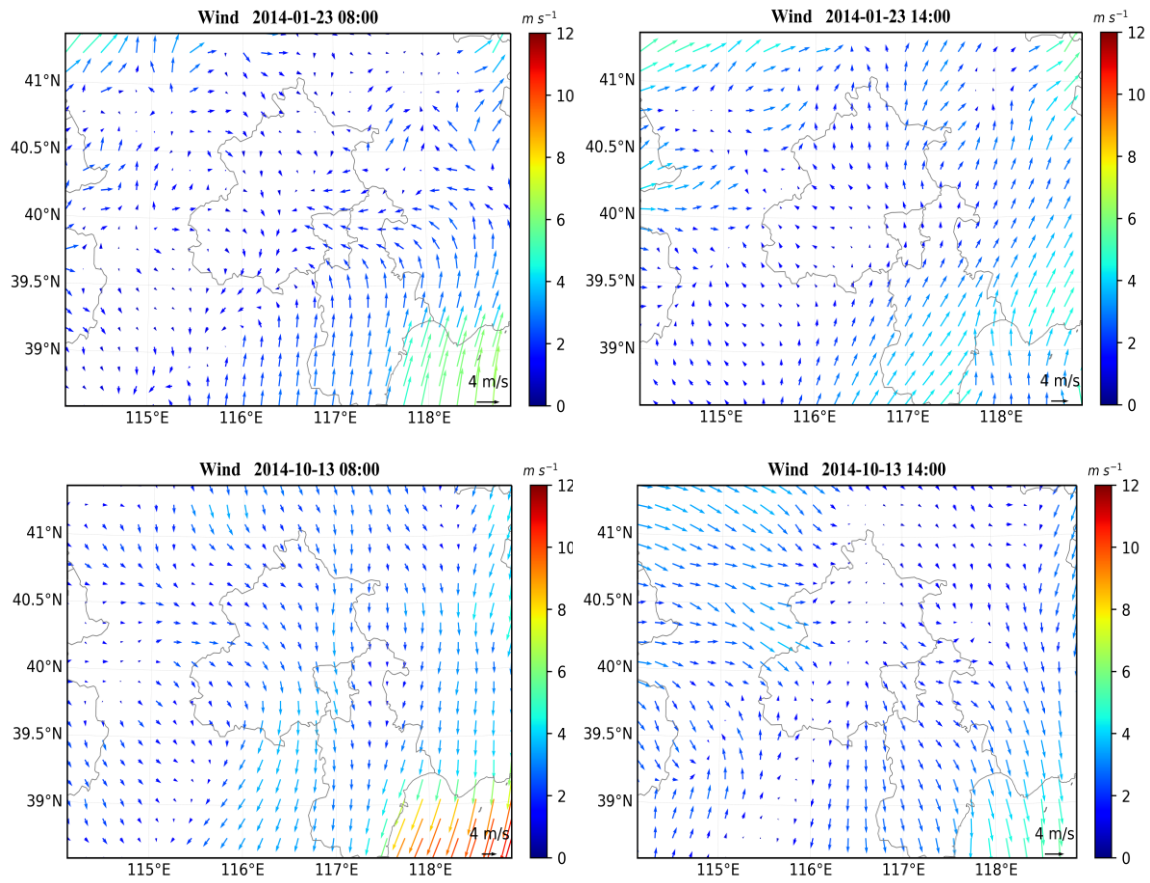


**Fig. 7** Wind fields in Beijing and the surrounding area from ECWRF at 08:00 (left column) and 14:00

(right column) BJT on January 23 and October 13, 2014.

1015

1020

1025

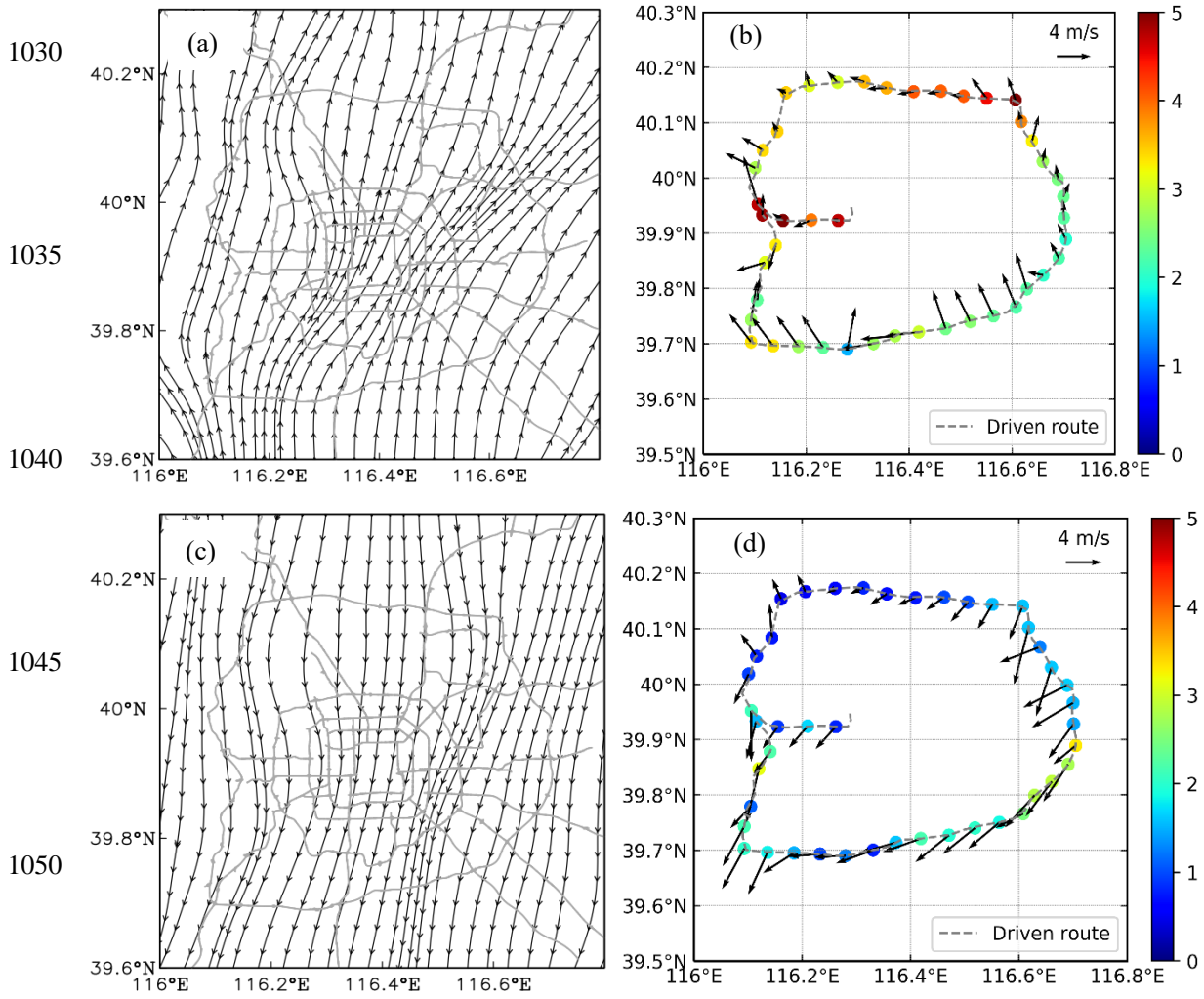


**Fig. 8** Average wind stream and NO<sub>2</sub> VCD ( $10^{16}$  molecules  $\text{cm}^{-2}$ ) distributions under the ~~three~~ two different types of wind field over Beijing: (a) south wind, (b) NO<sub>2</sub> VCD under south wind, (c) north wind, and (d) NO<sub>2</sub> VCD under north wind.

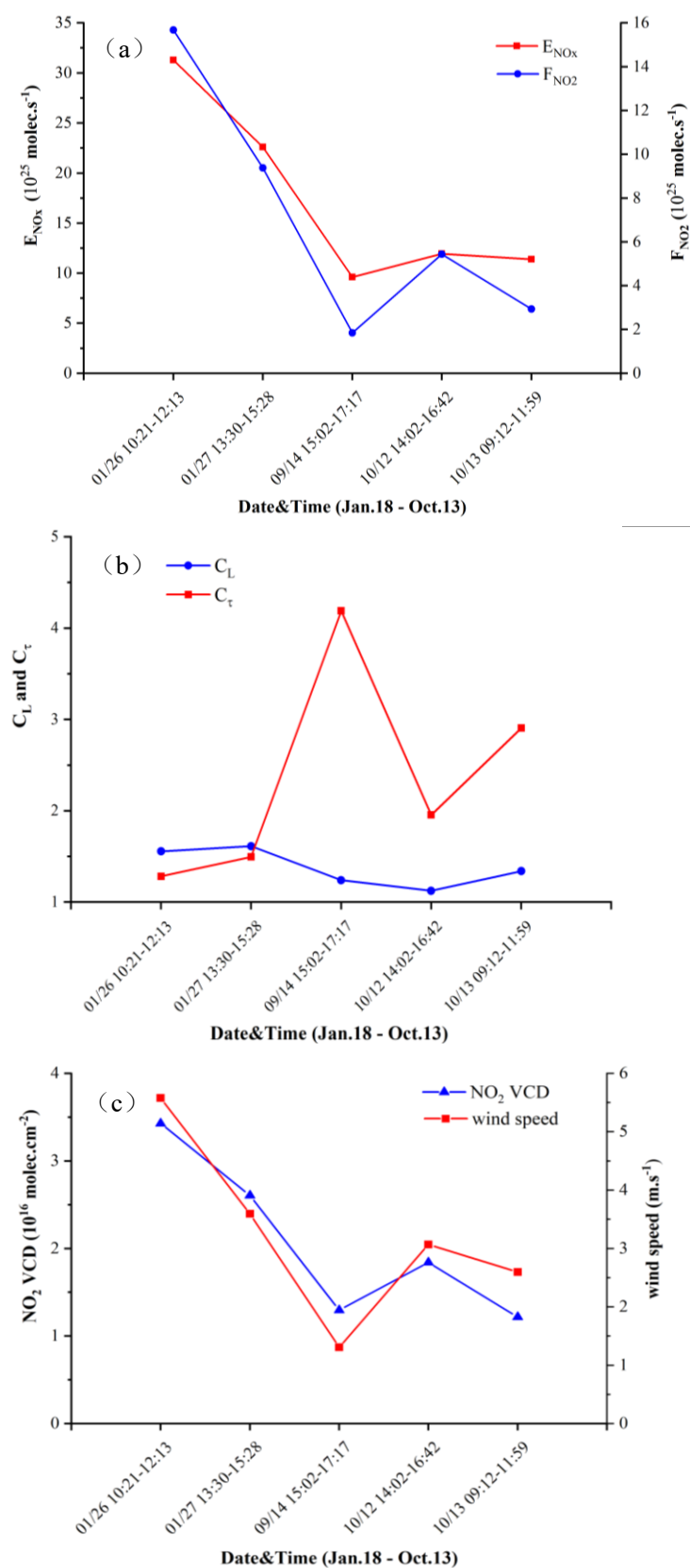


**Fig. 9** Journey-to-journey variations in (a)  $F_{NO_2}$  and  $E_{NOx}$ , (b)  $c_\tau$  and  $c_L$ , (c)  $NO_2$  VCD and mean wind speed for five circling journeys on the 6th Ring Rd of Beijing in January, September, and October, 2014.



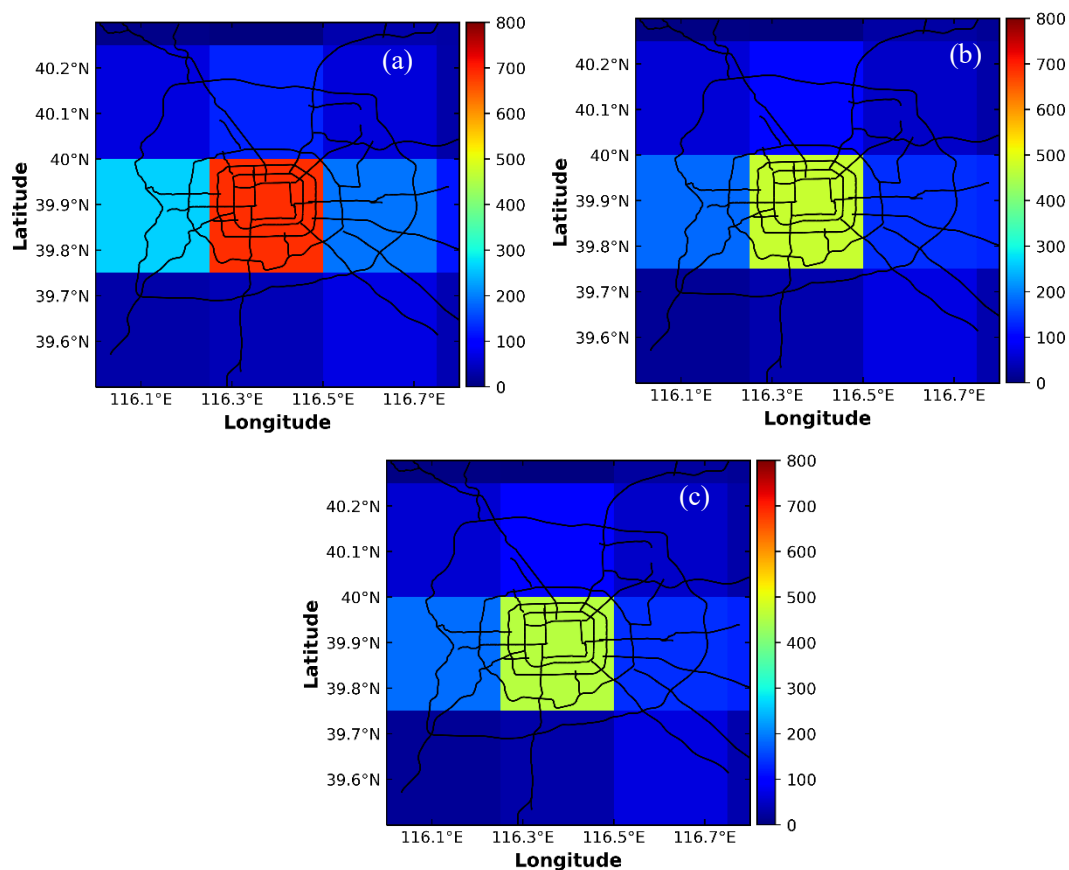


**Fig. 10** Spatial distributions of monthly averaged NO<sub>x</sub> emissions rate (mole km<sup>-2</sup> h<sup>-1</sup>) over Beijing based on the MEIC inventory in (a) January, (b) September, and (c) October in 2012.

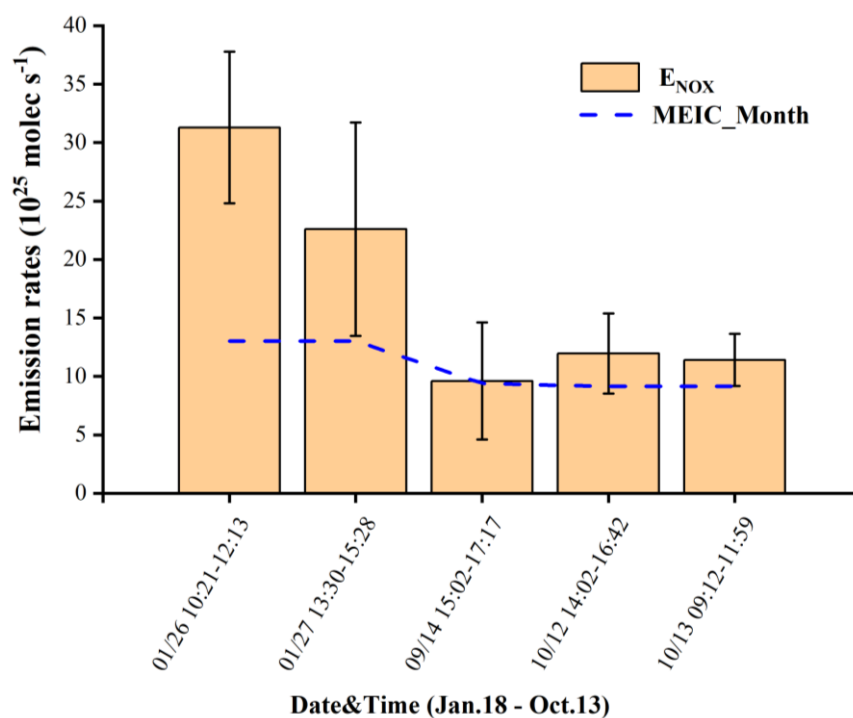


**Fig. 11** Journey-to-journey ~~variations~~ ~~variation~~ in estimated  $E_{NO_x}$  and corresponding monthly emissions ~~rate rates~~ from the MEIC inventory (MEIC\_Month) within the 6th Ring Rd of Beijing in January, September, and October 2014. Error bars represent the uncertainties in estimated  $E_{NO_x}$

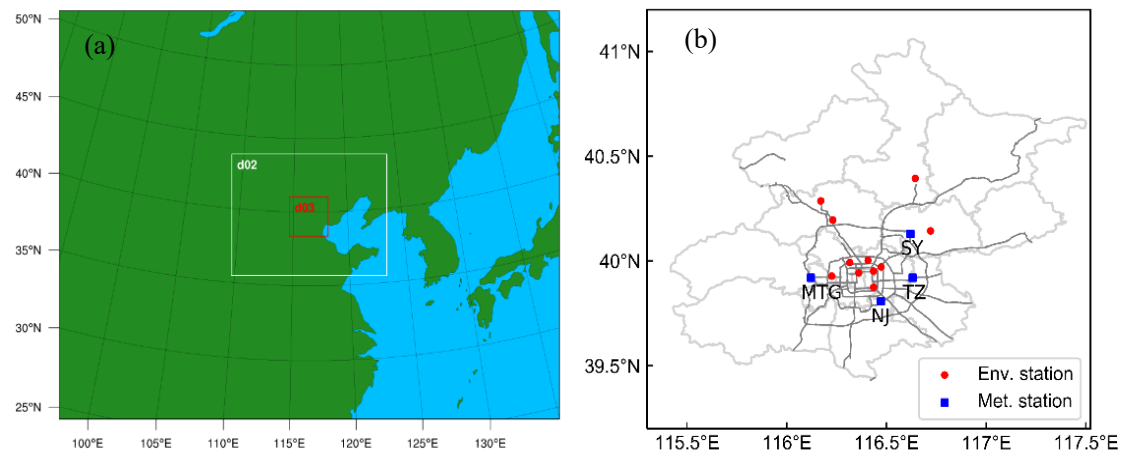


**Fig.S1 Fig.1S** Triple-nested domains of (a) the LAPS-WRF-CMAQ model system and (b) the distribution of meteorological/environmental monitoring stations.

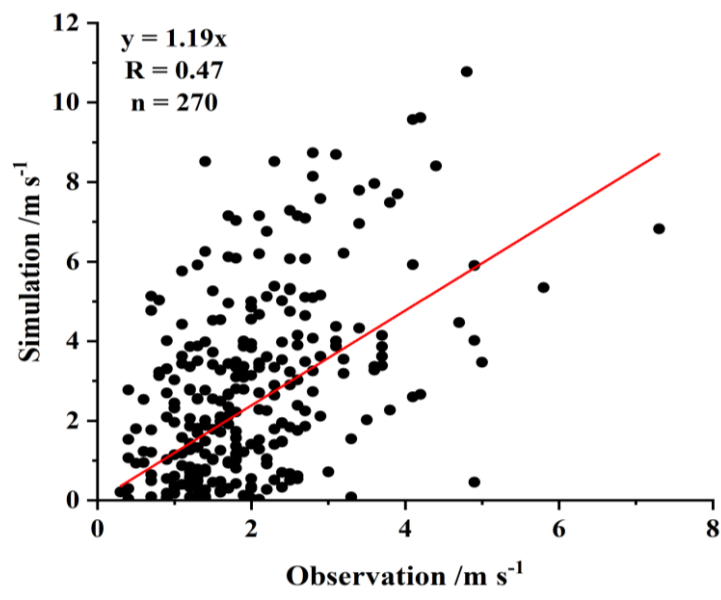


**Fig.S2 Fig.2S** Scatterplot of simulated wind speed and observations at four stations in Beijing. The standard deviation of the slope is 0.002.

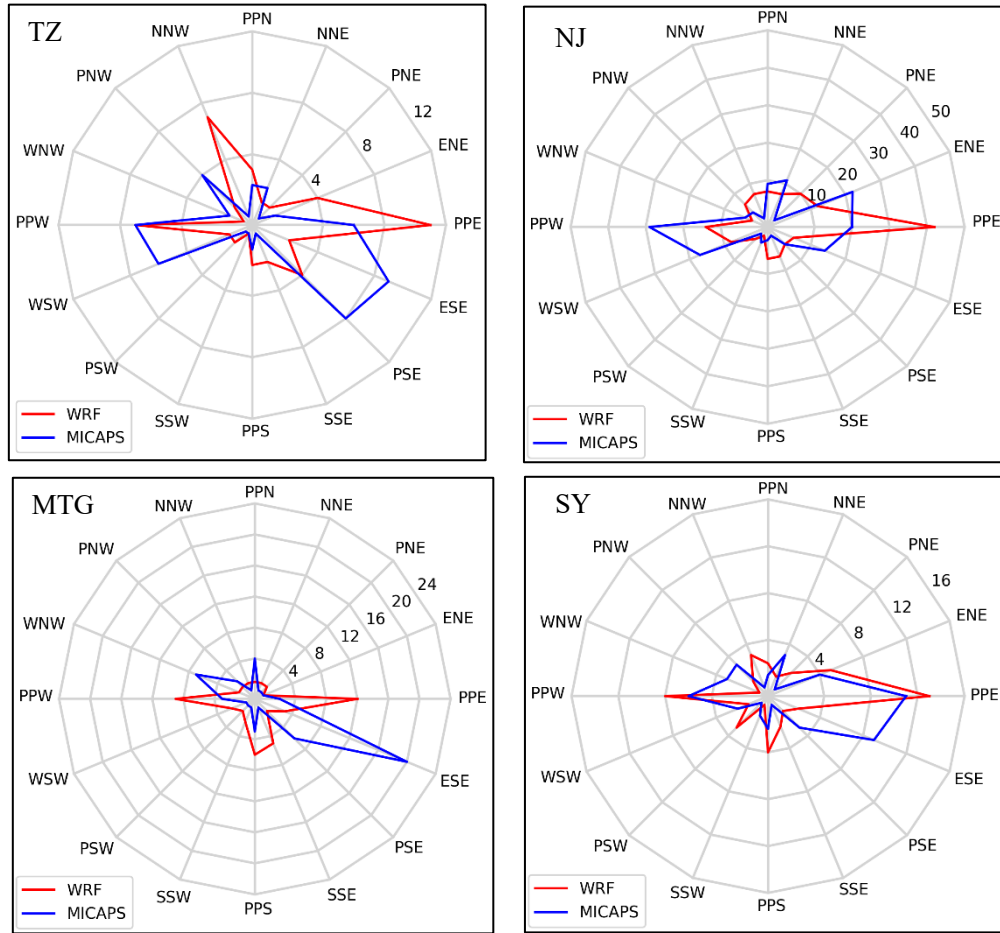


**Fig.S3Fig.3S** Wind rose of simulated wind direction and observations from MICAPS datasets at four stations in Beijing.

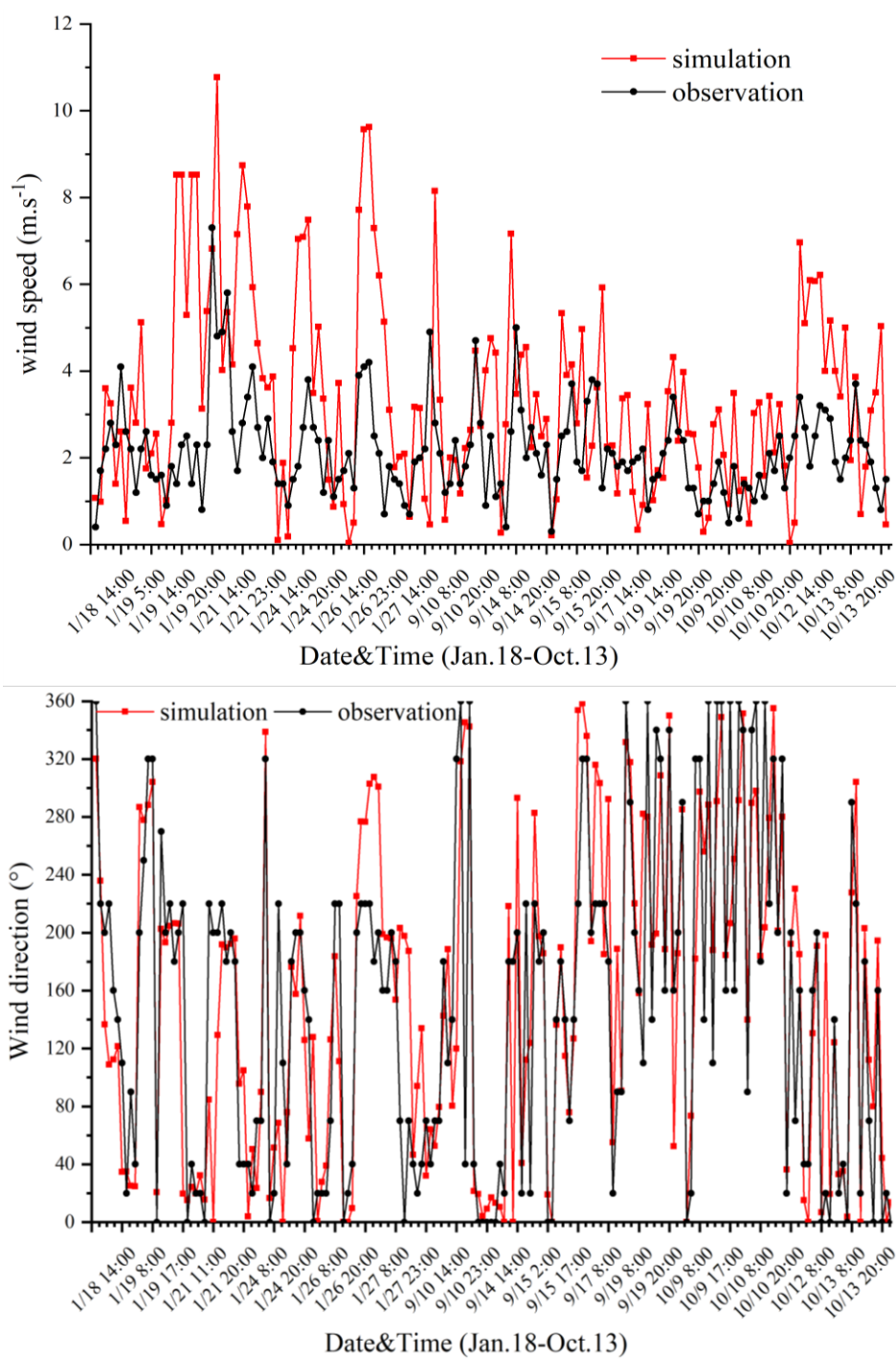


**Fig. S4** Time serial of simulated wind speed and direction, and observations during car MAX-DOAS experiments at four weather stations in Beijing.

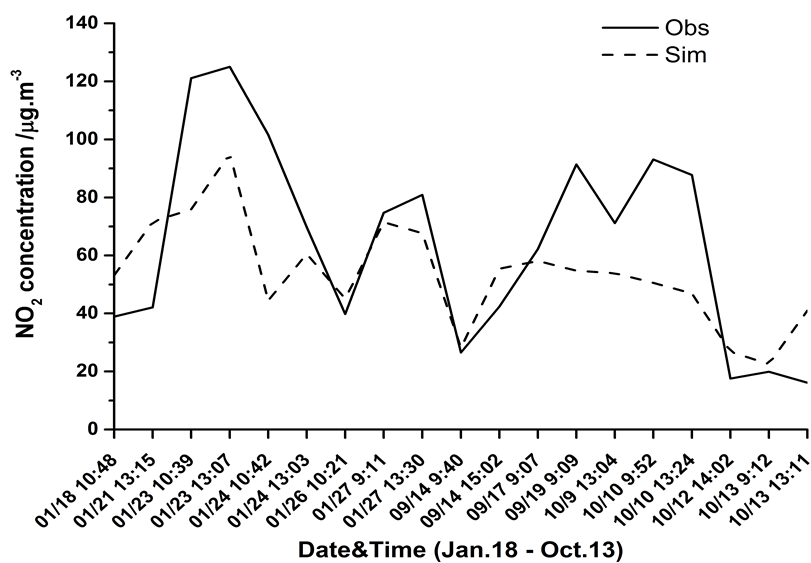


**Fig.S5Fig.4S** Time series of regional average simulation and in situ observation of NO<sub>2</sub> concentration at 12 stations in Beijing.

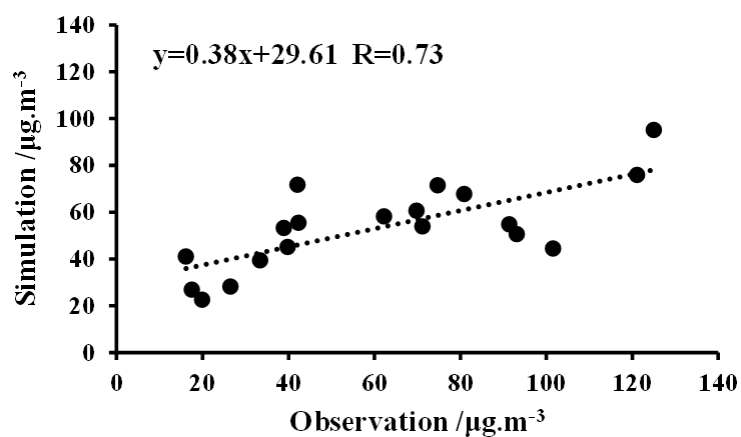


**Fig.S6Fig.5S** Scatter plot between regional average simulation and observation of NO<sub>2</sub> concentration at 12 stations in Beijing.

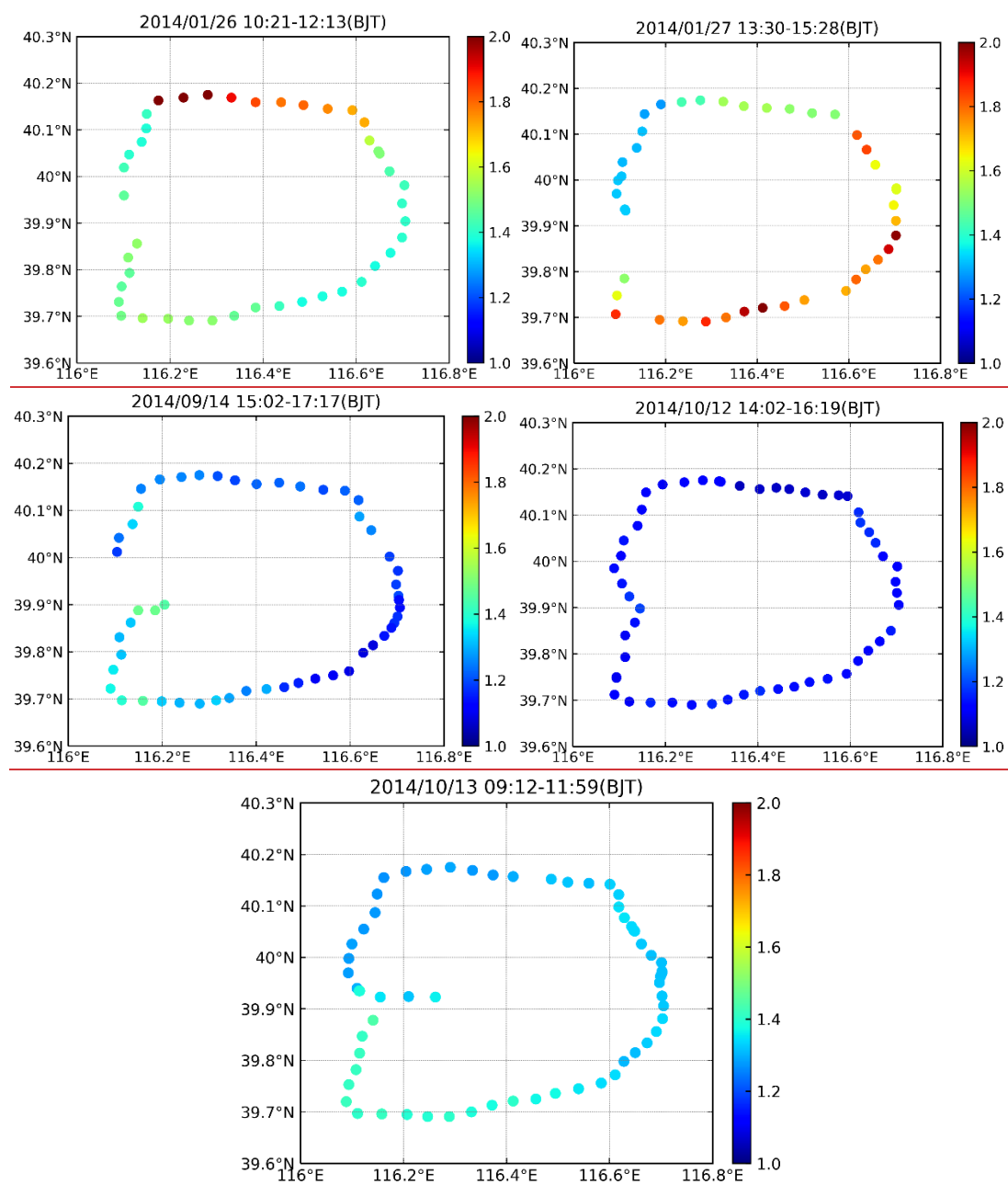


**Fig. S7** Distributions of the ratio of NO<sub>x</sub> and NO<sub>2</sub> on the 6th Ring Rd of Beijing during five journeys.

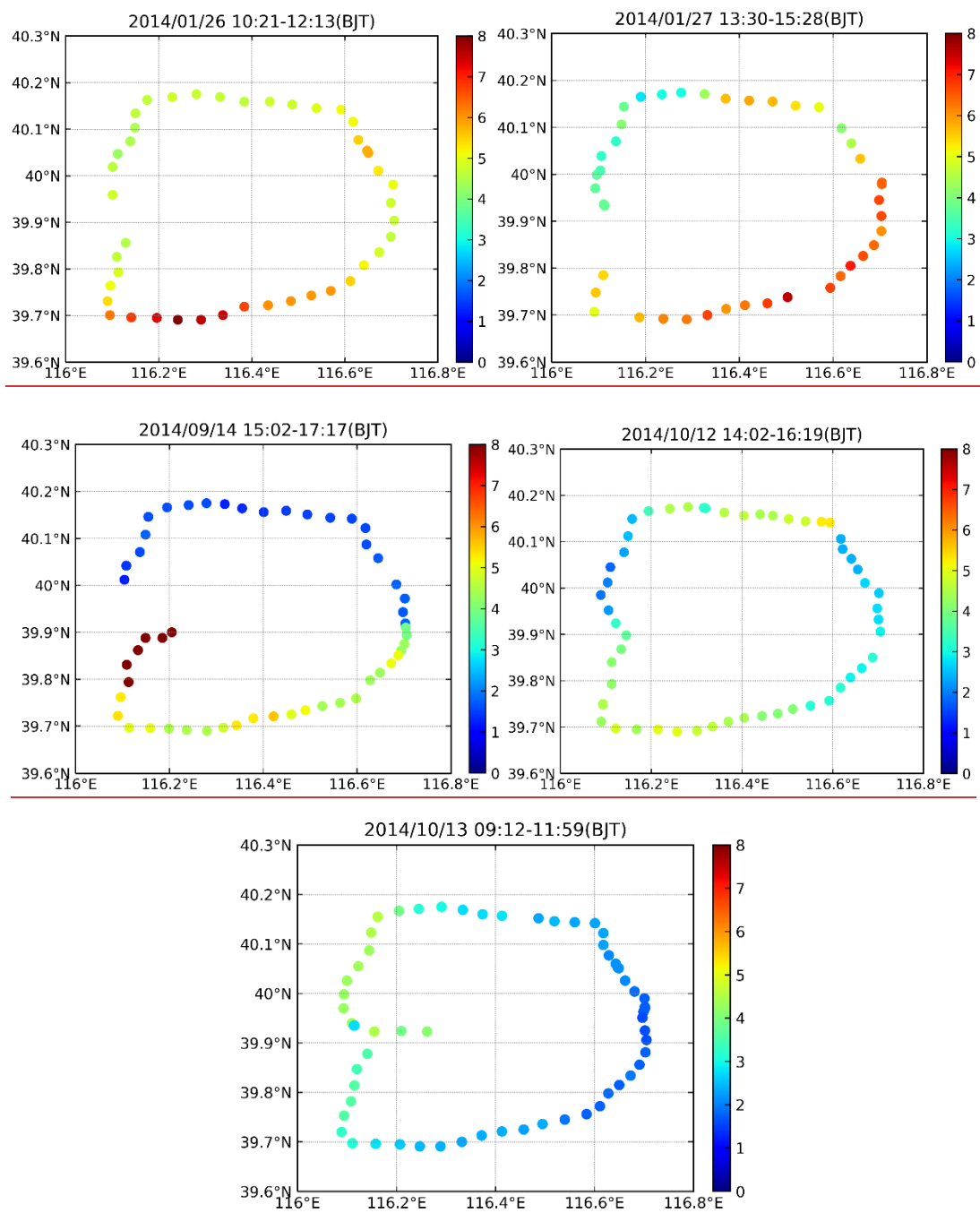


**Fig. S8** Same to figure S7, except for the lifetime of NO<sub>x</sub> (h).



Table S1. Four types of monthly  $E_{NOX}$  from the MEIC inventory within the 6th Ring Rd of Beijing in January, September, and October 2012, and the ratio of  $E_{NOX}$  in Jan. to the average in Sep. and Oct.

	<u>industry</u>	<u>power</u>	<u>resident</u>	<u>transport</u>	<u>total</u>
<u>January</u>	<u>5.78</u>	<u>1.92</u>	<u>1.39</u>	<u>3.94</u>	<u>13.02</u>
<u>September</u>	<u>4.06</u>	<u>1.15</u>	<u>0.25</u>	<u>3.93</u>	<u>9.40</u>
<u>October</u>	<u>4.03</u>	<u>0.93</u>	<u>0.26</u>	<u>3.93</u>	<u>9.15</u>
<u>Ratio</u>	<u>1.43</u>	<u>1.84</u>	<u>5.43</u>	<u>1.00</u>	<u>1.40</u>